APPLICATION OF PHOTOMETRIC ANALYSES FOR INTERPRETATION OF MARS-MARINER VI AND VII IMAGERY

Author: Robert E. Kinzly

CONTRACT NO. NASW-2222

Prepared For:

NATIONAL AERONAUTICS AND SPACE
ADMINISTRATION HEADQUARTERS
WASHINGTON, D.C. 20546

JULY 1977
CALSPAN REPORT VE-3104-M-1
FINAL TECHNICAL REPORT

Calspan Corporation
Buffalo, New York 14221

TABLE OF CONTENTS

LIST OF FIGURES

LIST OF TABLES

SECTION 1

INTRODUCTION AND SUMMARY

This is the final report under Contract NASW-2222 sponsored by the Planetary Geology Program at NASA Headquarter (Code SL). The objective of this program was to investigate and illustrate the application of radiometric analyses in the interpretation of Mariner VI and VII imagery. We felt that the following types of problems could be addressed using this imagery:

(1) Evaluation of local reflectivity changes,

(2) Augmentation of geologic mapping,

(3) Discrimination of atmospheric phenomena, and

(4) Investigation of polar cap structure.

The use of conventional radiometric techniques requires the ability to convert sensor response into surface radiance, that is radiometric calibration of the Mariner TV systems. In order to interpret the surface radiance, knowledge of the bi-directional reflectivity function and the atmospheric effects (if any) are required. To circumvent the requirement that these functions, i.e., the radiometric response and bi-directional reflectivity, be known with a high degree of accuracy an interpretation technique based upon reflectivity ratios was employed during this study. Alternate near encounter frames from the wide angle Mariner cameras were taken through different spectral filters (red, green or blue). Consequently, the overlap between successive frames show the same area of the martian surface in two spectral bands. We call these areas the bi-band coverage areas.

A comprehensive review of previous and subsequent efforts to the present study was made and is included in this report. In performing this survey it was obvious to us that the terminology and definitions employed in discussing radiometric investigations (both inter-planetary and earth-based) is quite divergent and confusing to the reader. This lack of precision makes the comparison of results difficult. Consequently the next section of this report proposes a radiometric model which incorporates the definitions and terms used in both astronomy and electro-optics.

As noted above, the interpretation of radiometric data can require knowledge of the bi-directional reflectivity or photometric function. Consequently in Section 2 we have reviewed the definition of this function and discuss several parametric models for its representation. We also have included the parametric values obtained by several authors in fitting observed radiometric data to the functional representations for Mars.

Section 3 reviews some of the radiometric analysis techniques employed in geology. The development of topographic information including crater distribution functions and topographic profiles, the use of global reflectivity in defining geologic units and in establishing surface composition and the interpretation of local reflectivity differences are discussed.

Our analysis on Mariner VI and VII imagery to interpret local variations in reflectivity by using reflectivity ratios is presented in Section 4. We identify the areas where bi-band spectral data is available

and present specific data in support of the interpretation methodology used. The results of our analysis show that light and dark markings interior to crater floors observed in Mariner frames 6N11 and 6N13 acquired through green and red filters respectively are caused by differences between particle sizes between the dark and light areas. Based upon laboratory spectral reflectivity data the most likely size groups for the particles in the two areas is consistent with that proposed by others. Global reflectivity differences between dark and light areas obtained by other authors support larger particle size differences. Based upon our data and that provided by other authors, we concluded that the most likely composition of this local area is limonite stained pyroxene, the latter being a basic silicate common in meteorites. Despite the evidence for basaltic flows on Mars, olivine which is associated with such flows was ruled out as a major constituent in this area based upon its relatively high normal reflectivity.

The application of reflectivity ratio analysis to geologic mapping and the study of atmospheric phenomena was inhibited by the limited amount of data available. It was anticipated that the Mariner IX mission would provide a wealth of bi-band coverage areas on the martian surface and analysis of this data was anticipated. Unfortunately the filter wheel became inoperative on Revolution 118 subsequent to the subsiding of the global martian dust storm. As a consequence, no significant bi-band coverage area of the martian surface was obtained during the Mariner IX mission and this portion of the study was deleted.

SECTION 2

THE RADIOMETRIC MODEL

While the primary objective of this study was not the development of basic radiometric (or photometric) principles or techniques but their application to planetology, an understanding of these principles had to be achieved in order to assess the efforts of related research. Unfortunately, the historical development of radiometric science in astronomy and in electro-optics has not had complete commonality--leading to a diversity of definitions and structure that can be confusing to the engineer not versed in both disciplines. This can result in the misinterpretation of the data presented in other research efforts. Nicodemus (1967) has noted:

> "Radiometry and particularly its overshadowing subdivision, photometry, are embarrassed by diversity in nomenclature. Careful attention to the definitions of all radiometric terms, symbols, and units both by authors and readers is needed to avoid confusion and misunderstanding."

In this section of our report we present a proposed radiometric model and provide definitions that include concepts from both astronomical and electro-optical radiometry as a basis for standardization in this and future efforts in terrestial geology as well as planetology.

An important distinction is made depending on the spectral response of the detector in radiometry. Terms such as luminance, illuminance and brightness are used in photometry where the detector has a spectral passband equal to that of the eye (photopic response). Although this is quite precise the prefix "photo" is frequently used when this is not the case.

An example in astronomy and planetology is the definition of "photometric function" which can be measured over a narrow visible or IR spectral band and is rarely measured with a photopic response. The model and terminology presented below is based upon a summary of radiometry (Nicodemus, 1967).

The geometry of the incident and reflected light from a planar surface (in the x-y plane) is shown in Figure 1. Reflectance of an opaque surface is a function of the influx direction through angles θ_i and ϕ_i and the efflux direction through angles θ_r and ϕ_r. The basic quantity

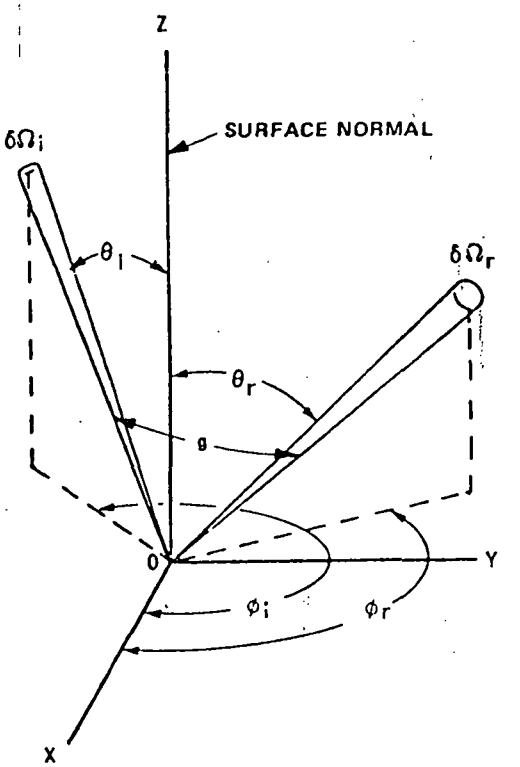

Figure 1. RADIOMETRIC MODEL GEOMETRY

is the spectral radiance, $N_\lambda(\theta_i, \phi_i, \theta_r, \phi_r)$, emanating from the surface and is expressed in units watts/$m^2 \cdot sr \cdot \mu m$. The wavelength dependence is removed by integrating over the bandwidth of the incident light and the spectral response of the detector. The explicit dependence on wavelength is suppressed below with the understanding that the terms imply a particular bandpass.

The reflectance (dimensionless) of the surface is defined as the ratio of the reflected radiant power to the incident radiant power

$$\rho \equiv \frac{P_r}{P_i} = \frac{\int N_r(\theta_r, \phi_r)\, d\Omega'_r}{\int N_i(\theta_i, \phi_i)\, d\Omega'_i} = \frac{\int N_r(\theta_r, \phi_r)\, d\Omega'_r}{H_i(\theta_i, \phi_i)} \qquad (1)$$

where the projected solid angle $d\Omega' = \sin\theta \cos\theta\, d\theta\, d\phi$. Both the incident radiance N_i and the reflected radiance N_r are functions of their respective direction angles (θ, ϕ). The reflectance of the surface as defined above can change as the receiver geometry is changed. Clearly we do not generally want to adopt such a definition. An exception occurs when the detector measures all of the reflected radiation, i.e., that reflected into the hemisphere, in which case we obtain the diffuse reflectivity or the Bond albedo discussed below.*

The reflecting properties of the surface are more appropriately described by the bidirectional reflectance function defined by

*The term reflectivity implies decimal fraction while reflectance is expressed in percent. For historical interest we note that the Bond albedo was introduced in 1861.

$$\rho'(\theta_i,\phi_i,\theta_r,\phi_r) \equiv \frac{N_r(\theta_r,\phi_r)}{H_i(\theta_i,\phi_i)} \tag{2}$$

where $H_i(\theta_i,\phi_i)$ is the incident irradiance in watts/m^2. Note that ρ' has dimensions of steradians^{-1}. Combining equations (1) and (2) the diffuse reflectivity (or Bond albedo) is given by:

$$\rho_d = \frac{\int_h \rho'(\theta_i,\phi_i,\theta_r,\phi_r) H_i(\theta_i,\phi_i)\, d\Omega'_r}{H_i(\theta_i,\phi_i)} = \int_h \rho'(\theta_i,\phi_i,\theta_r,\phi_r)\, d\Omega'_r \tag{3}$$

where "h" signifies integration over the hemisphere. For a perfectly diffuse (Lambertian) surface ρ' is independent of receiver coordinates and

$$\rho_d = \rho' \int_h d\Omega'_r = \pi \rho' \tag{4}$$

The normal reflectivity (or normal albedo), ρ_o, is the value of the bidirectional reflectance function when $\theta_i = \theta_r = 0$ and the influx and efflux directions are both normal to the surface:

$$\rho_o = \frac{N_r(0,0)}{H_i(0,0)} \tag{5}$$

In practice the normal albedo can be computed by measuring the radiance of the center of the planet (or the sub-earth point) near opposition and calculating H_i.

If we normalize the bidirectional reflectance to 1.0 at zero influx and efflux zenith angles Equation (2) becomes:

$$\rho'(\theta_i,\phi_i,\theta_r,\phi_r) = \rho_o \Phi(\theta_i,\phi_i,\theta_r,\phi_r) \tag{6}$$

where Φ is the normalized function. In planetology and astronomy Φ is referred to as the photometric function even though it can be measured over non-photopic spectral bandpasses. In radiometric terms it is the normalized bidirectional reflectivity. The diffuse reflectivity (Bond albedo) can now be expressed in terms of the normal albedo, namely

$$\rho_d = \rho_o \int_h \Phi(\theta_i,\phi_i,\theta_r,\phi_r)\, d\Omega'_r \tag{7}$$

where the integral is referred to as the phase integral.

Retroreflectivity (or geometric albedo) is the value of the bi-directional reflectivity when the influx and efflux angles are equal (zero phase angle), but not necessarily zero themselves, namely

$$\rho_r(\theta) = \rho_o \Phi(\theta,\phi,\theta,\phi) \tag{8}$$

Note that the normal reflectivity is a special case of the retroreflectivity. The geometric albedo accounts for the variation in apparent brightness across a planetary disk near opposition. Because the lunar disk appears to be uniform, i.e. no limb darkening, its retroreflectivity is constant and equal to its normal reflectivity. This is not true for the martian disk where limb darkening effects have been observed. Frequently the terms normal albedo and geometric albedo are used interchangeably leading to some confusion. The average reflectivity of a planetary disk near

opposition is an area weighted average of its retroreflectivity or geometric albedo but is sometimes identified as the geometric albedo of the planet.

In many situations the bidirectional reflectivity, Eq. (2), is not a function of the four angles $(\theta_i, \phi_i, \theta_r, \phi_r)$ but only three (θ_i, θ_r, g) where g is the phase angle shown in Figure 1.* This allows the bidirectional reflectivity to be written as:

$$\rho'(\theta_i, \theta_r, g) = \frac{N_r(\theta_r, g)}{H_i(\theta_i)} = \rho_o \Phi(\theta_i, \theta_r, g) \qquad (9)$$

This simplification is a consequence of <u>assumed</u> symmetry properties of the material, e.g. that the reflectivity is independent of a rotation about its normal. Although most radiometric ("photometric") studies of planetary surfaces accept this assumption it may not always be valid--for example if wind blown dust were to have a preferential deposition $\Phi(\theta_i, \theta_r, g)$ could be ambiguous.

Finally using the more conventional notation, $\theta_i = i$ and $\theta_r = \epsilon$, the component of radiance due to a planetary surface is given by the expression:

$$N(i, \epsilon, g, \lambda) = S(i, \lambda)\, t(\epsilon, \lambda)\, \rho_o(\lambda)\, \Phi(i, \epsilon, g, \lambda) \qquad (10)$$

where $S(i,\lambda)$ is the irradiance on the surface at wavelength λ and $t(\epsilon,\lambda)$ is the

*Note that $|\theta_i - \theta_r| \leq g \leq \theta_i + \theta_r$

loss factor due to the transmissivity of the optical path. Note that in the presence of a significant atmosphere S will include both solar and sky components and that the apparent radiance of the planet will include an atmospheric component as well as a surficial component. For the moon, Mercury and Mars (except during dust storms) the surficial component dominates the observed radiance.

Unfortunately one of the other ambiguities in the definition of radiometric terms is that factors of π "come-and-go". Some authors may have a factor of $1/\pi$ multiplying the right side of Eq. (10). This factor originates because of a difference in the definition of photometric units between the English and metric systems. To further complicate the situation, a similar difference does not formally exist for radiometric units although many authors impose such conditions in order to use operationally measured reflectivities. The English units were developed to facilitate the operational measurement of reflectivity such that a perfectly reflecting diffuse (Lambertian) surface has a bidirection reflectivity of unity. The English unit of luminance (ft-Lambert) has been rationalized by a factor of π in addition to the conversion factor from m^2 to ft^2. Consequently the luminous bidirectional reflectivity, Eq. (2), is increased by π, viz: $\rho' = \pi N_R/H_i$ and the diffuse reflectivity, Eq. (4), becomes $\rho_d = \rho'$ (i.e. the bidirectional reflectivity of a Lambertian surface is numerically equal to its diffuse reflectivity) and the factor of $1/\pi$ enters Eq. (10). Note also that $N_r(\theta_r, \phi_r)$ is constant for a Lambertian surface and the definition based upon the ratio of reflected to incident power, Eq. (1) also becomes $\rho = \pi N_r/H_i$ and the two definitions of luminous reflectivity are identi-

cal for Lambertian surfaces. Operationally we frequently measure the bidirectional reflectivity of a material by comparing the received power to that received from a Lambertian standard (with $\rho_d \simeq 1.0$) at the same orientation, the value obtained is governed by the alternate definition discussed here and the multiplying factors discussed above apply.

SECTION 3

BIDIRECTIONAL REFLECTIVITY (PHOTOMETRIC) FUNCTION

It is clear from the results of the previous section that some knowledge of the bidirectional reflectivity characteristics of the surficial materials on a planet are required in order to interpret the radiance measured by either an imaging system or a radiometer. Even if a planetary surface were composed of a single type of material with a well defined particle size regime, the radiance of the planetary surface will vary due to geometrical considerations alone. Both the normal reflectivity and the normalized bidirectional reflectivity (photometric) function can change due to compositional differences on the planetary surface. Consequently, it becomes a matter of removing the geometrical dependence of the radiance to arrive at an "albedo" which contains information about the composition of the surface. One approach is to use Eq. (10) to convert the observed radiance into the normal albedo. This requires knowledge of the normalized bidirectional reflectivity or photometric function. The normal albedo differences subsequently derived can be due to chemical or mineralogical differences, particle size differences or a combination of these effects. A primary objective of this study was to determine whether observed albedo differences (dark and light markings) in Mariner VI and VII photography of the Martian surface were due to chemical effects or particle size differences. However the analyses methodology did not require the computation of the normal albedo or reflectivity.

If we assume that there are no chemical or composition differences then the photometric function or normalized bidirectional reflectivity can be derived from measurements of the radiance of the surface at different illumination and viewing conditions. The measured data is fit to an analytic model for the photometric function. The most frequently used functional representation for surface radiance is the Minnaert equation (Minnaert, 1941). This equation is a parametric expression developed to obey the Helmholtz reciprocity law -- the bidirectional reflectivity is invariant upon reversability of the incident and emission angles, namely

$$\rho'(i,\epsilon,g) = \rho'(\epsilon,i,g) \tag{11}$$

The resulting parametric equation has the form

$$N(i,\epsilon,g,\lambda) = N_p(g,\lambda)\,(\cos i)^{k(g,\lambda)}(\cos\epsilon)^{k(g,\lambda)-1} \tag{12}$$

where the exponential parameter, k, is a function of both the phase angle and wavelength and can be thought of as a limb darkening parameter. The moon, which has no limb darkening effect, has a value of k=0.5 at zero phase while a Lambertian surface would have a value of k=1.0. The Minnaert law is frequently written with the symbol "B" in place of the symbol "N" which we have employed. The former implies the brightness of the surface in contrast to the radiance and consequently in keeping with the discussion in Section 3 we have avoided its use here. The term $N_p(g,\lambda)$, frequently written as "B_o" can be a function of phase angle without violating the reciprocity requirement

since it does not depend on the incident or emission angle. At zero phase note that N_p is equal to the radiance obtained at normal incidence and normal emission, namely $N_p(0,\lambda)=N_r(0,0)=H_o(\lambda)\rho_o$ where H_o is the irradiance at normal incidence. This is required so that Eq. (12) has the correct limit at $i=\epsilon=0$. The Minnaert equation is frequently used in a modified form obtained by implicitly dividing both sides by $H_o(\lambda)$. In this case the value of the parameter N_p or B_o at zero phase angle is the normal reflectivity or albedo. If we assume that N_p is not a function of the phase angle, then $N_p \equiv H_o(\lambda)\rho_o$ for the reasons given above. Some authors make this assumption without noting that it may not be justified.

Comparing Eq. (12) to Eq. (10) and assuming that the loss due to the atmosphere is negligible, the photometric function described by the Minnaert equation is

$$\Phi(i,\epsilon,\xi,\lambda) = \frac{N_p(\xi,\lambda)}{H_o(\lambda)\rho_o(\lambda)} (\cos i)^{k(\xi,\lambda)-1} (\cos\epsilon)^{k(\xi,\lambda)-1} \qquad (13a)$$

Equating the photometric function and the Minnaert equation, the practice of some authors, is somewhat imprecise and misleading. If N_p is not a function of the phase angle the photometric function becomes

$$\Phi(i,\epsilon,\xi,\lambda) = (\cos i)^{k(\xi,\lambda)-1} (\cos\epsilon)^{k(\xi,\lambda)-1} \qquad (13b)$$

The Far Encounter photography obtained during the Mariner VI and VII missions has been employed to estimate the parameters N_p,k in Equations (12) and (13) (Young, 1971). The video signal was converted to reflectivity using available calibration data such that the value of N_p/H_o at zero phase would be the normal reflectivity (albedo), ρ_o, if it could have been estimated. Log-log plots of $N \cos \epsilon$ versus $\cos i \cos \epsilon$ called "Minnaert plots" were constructed to estimate N_p/H_o and k. Since these photographs were obtained with the long focal length TV camera and occurred at limited phase angles, $\sim 23^o \pm 2^o$ this evaluation did not include the variation of N_p/H_o or k with phase angle or wavelength. The results obtained from each of the missions are summarized in the table below. The variation of k from place to place on Mars was attributed to a variation in composition and supported the hypothesis that the Martian surface is more than a two-component system.

Table 1

Minnaert Parameters from Mariner VI and VII Imagery

Region	West Longitude, deg.	Latitude, deg.	k_6	k_7	$\frac{N_{p6}}{H_o}$ Ster^{-1}	$\frac{N_{p7}}{H_o}$ Ster^{-1}
Ophir	68	-8	0.63	0.71	0.146	0.131
Center of Elysium	213	+12	0.56	0.55	0.144	0.132
Aeolis	213	0	0.61	0.68	0.133	0.133
Center of Syrtis Major	290	+5	0.46	0.48	0.093	0.071
Solis Lacus	90	-40	0.66	0.60	0.117	0.093

Earth-based observations of the radiance of Mars have also been employed to estimate the parameter k (Binder, 1972). Unfortunately Earth-based observations are constrained in that measurements cannot be made of the Martian surface at phase angles greater than 40° due to ephemeris considerations. The results of these measurements show a slightly higher value of k at a 23° phase angle, namely $k \approx 0.8$. These data were measured at a wavelength of $0.60\,\mu m$. The differences between these two measurements of k are most likely the result of the differences in the spectral bandpass of the sensors. This study also evaluated the variation of k with wavelength with the resulting dependence at approximately 10° phase angle.

$$k(10^{\circ}, \lambda) = 0.91 - .16/\lambda \qquad (14)$$

Since the spectral passband of the B camera varies from $0.48\mu m$ to approximately $0.65\,\mu m$ (Danielson, 1971) the value of the k parameter according to Eq. (14) corrected for the phase angle difference would vary from 0.74 to 0.84, still somewhat higher than the Mariner derived values. We note, however, that Binder arbitrarily assumed that k at zero phase angle was 0.5 (no limb darkening effect).

A more recent evaluation of the Minnaert coefficients derived from observations on the Mariner IX imagery (Thorpe, 1973) resulted in values presented in Table 2 as a function of phase angle at an effective wavelength of $0.56\,\mu m$. In this case also the value of N_p at zero phase would be the normal reflectivity. Note that the results presented in the table clearly indicate that N_p is dependent on the phase angle. If we fit results of

Table 2

Minnaert Parameters from Mariner IX Imagery

Phase (deg)	20	30	40	50	60	70	80
N_g	0.166±0.02	0.156±0.30	0.145±0.03	0.14±0.02	0.132±0.03	0.129±0.03	0.135±0.04
k	0.70 ±0.01	0.73 ±0.06	0.77 ±0.03	0.80±0.02	0.84 ±0.05	0.87 ±0.04	0.91 ±0.05

Thorpe for the variation of k with phase angle with a linear equation we find that

$$k(g) = 0.63 + 0.0035\ g \qquad (15)$$

since $k(0) > 0.5$ this indicates a limb darkening effect on Mars.

Measurements of the Minnaert coefficient k at a mean phase angle of 58^{o} were also made during the initial portion of the Mariner IX mission while a dust storm covered Mars (Masursky et al, 1972). For these measurements k increased from 0.93 to 1.12 with increasing wavelength and indicate a nearly Lambertian surface (k=1.0). This result would be expected for an optically thick atmosphere composed of small particles ("dust").

A recent research effort has led to an alternative expression for the photometric function (Meador, 1975). Although more complex than the Minnaert law the Meador equation has the distinct advantage that its parameters can be related to the physical characteristics of the reflecting surface, e.g. particle size, single-particle albedo and compactness. The explicit functional form will not be presented here and the interested reader is referred to the cited reference for details. This expression has been compared to the three data sets previously used to derive the parameters for the Minnaert law as discussed above (Weaver, 1974). Based upon the fit of the Meador expression to the experimental observations and laboratory data on Colorado Basalt it was concluded that the mean intercenter spacing

of adjacent particles is about 4/3 of the mean diameter. The mean diameter was concluded to be greater than 225 μm and not in conflict with other indications that the mean diameter of Martian surface particles is about 400 μm.

Regardless of which expression is used to represent the bidirectional reflectivity or photometric function in order to analyze the radiance of a planetary surface as measured by either an imaging system or a radiometer, the values of the influx or incident angle, i, the efflux or emission angle, ϵ, and the phase angle, g, must be determined. If the latitude and longitude of the sub-solar point are known (ϕ_{sz}, λ_{sz}) the incident angle at a point having latitude and longitude (ϕ, λ) is given by

$$\cos i = \sin\phi \sin\phi_{sz} + \cos\phi \cos\phi_{sz} \cos(\lambda - \lambda_{sz}) \qquad (16)$$

The sub-solar point is the location on the planetary surface where the line from the center of the sun to the center of the planet intersects the surface. Similarly if the sub-spacecraft point is known (ϕ_{ss}, λ_{ss}) the emission angle can be determined by using

$$\cos\epsilon = \sin\phi \sin\phi_{ss} + \cos\phi \cos\phi_{ss} \cos(\lambda - \lambda_{ss}) \qquad (17a)$$

As the spacecraft approaches the planet a (parallax) correction may be required. The emission angle, ϵ, given by Eq. (17a) is increased by δ.

$$\tan\delta = \sin\epsilon / (R_s/r - \cos\epsilon) \qquad (17b)$$

where ϵ is the value determined from Eq. (17a), R_s is the distance from the spacecraft to the center of the planet and r is the radius of the planet. For the Mariner VI and VII imagery the values of R_s have been computed by Davis (1971) and $r \pm 3385$km for Mars. For the Mariner VI and VII imagery $R_s/r = 2\text{-}3$ and the correction factor is significant. The locations of the sub-solar and sub-spacecraft paints are not as readily documented and must be determined from orbital data. If the azimuth angle between the incident and emission planes is known and equal to θ then the phase angle is given by

$$\cos g = \cos i \cos\epsilon + \sin i \sin\epsilon \cos\theta \tag{18}$$

The angle θ is the difference between the bearing of the sub-solar point, Z_{sz},

$$\cos|z_{sz}| = \frac{\sin\phi_{sz} - \cos i \sin\phi}{\sin i \cos\phi} \tag{19a}$$

and the bearing of the sub-spacecraft point, Z_{ss},

$$\cos|z_{ss}| = \frac{\sin\phi_{ss} - \cos\epsilon \sin\phi}{\sin\epsilon \cos\phi} \tag{19b}$$

The sign of Z_{sz} and Z_{ss} is determined by the value of the longitudes $\lambda_{sz}, \lambda_{ss}$ with respect to λ.

SECTION 4

RADIOMETRIC APPLICATIONS IN GEOLOGY

In this section we discuss some of the applications of radiometry and the bidirectional reflectivity function in obtaining information about the geology of planets. No attempt has been made to make this discussion exhaustive but only representative of some of the applications available. The discussion has been divided into three categories which include (1) the influence of reflectivity on topographic information, (2) the use of reflectivity for global geology, and (3) the use of local changes in reflectivity in assessing compositional differences in surficial material.

4.1 Topographic Applications

Two examples where the reflectivity characteristics of a planetary surface influences topographic information include the use of imagery in crater distribution studies and the development of topographic profiles from photometrically corrected image data.

The effect of the finite resolution of an imaging sensor (e.g., Mariner television systems) upon the accuracy of distribution data is well known, namely as the diameter of the crater approaches the resolution limit of the imaging system the measured distribution falls below the actual distribution due to the inability to identify and measure the craters on the reconstructed imagery. The reflectivity characteristics of the planetary surface play a role in how rapidly the loss of information due to limited

resolution occurs. This point is not necessarily appreciated by all investigators utilizing the imagery in obtaining their photogrammetric information. The resolution of an imaging system is most often quoted assuming that the object being imaged is high contrast (having extreme radiance values). As the contrast of the object decreases the resolution limit becomes poorer. That is, the inherent resolution limit of the imaging system is only achieved under illumination and viewing conditions where the objects under study have a reasonably high contrast. At high phase angles most surface features have associated shadows which enhance their contrast. Consequently, one would expect the information content of imagery acquired at large phase angles to be higher than that acquired at lower phase angles. As part of the development of quality evaluation techniques for Lunar Orbiter photography the author (Kinzly, 1967) developed an expression for information content in terms of a number of mission parameters including phase angle which was subsequently related to the minimum detectable crater diameter of Lunar Orbiter photography. The variation of the minimum crater diameter with respect to phase angle for this photography is shown in Figure 2. A 4:1 variation occurs as the phase angle changes from 0 to 90^{o}. The change is most dramatic in the region from 60^{o} to 90^{o} emphasizing the value of large phase angle photography. More recently the importance of illumination conditions upon comparative planetary geology has been evaluated (Schultz, 1976). Comparative geology uses imagery from several planetary and lunar missions. It is noted, for example, that the information content of the Mariner IX imagery is comparable to the Mariner VI and VII imagery despite the smaller slant ranges involved on the former mission. The improved theoretical

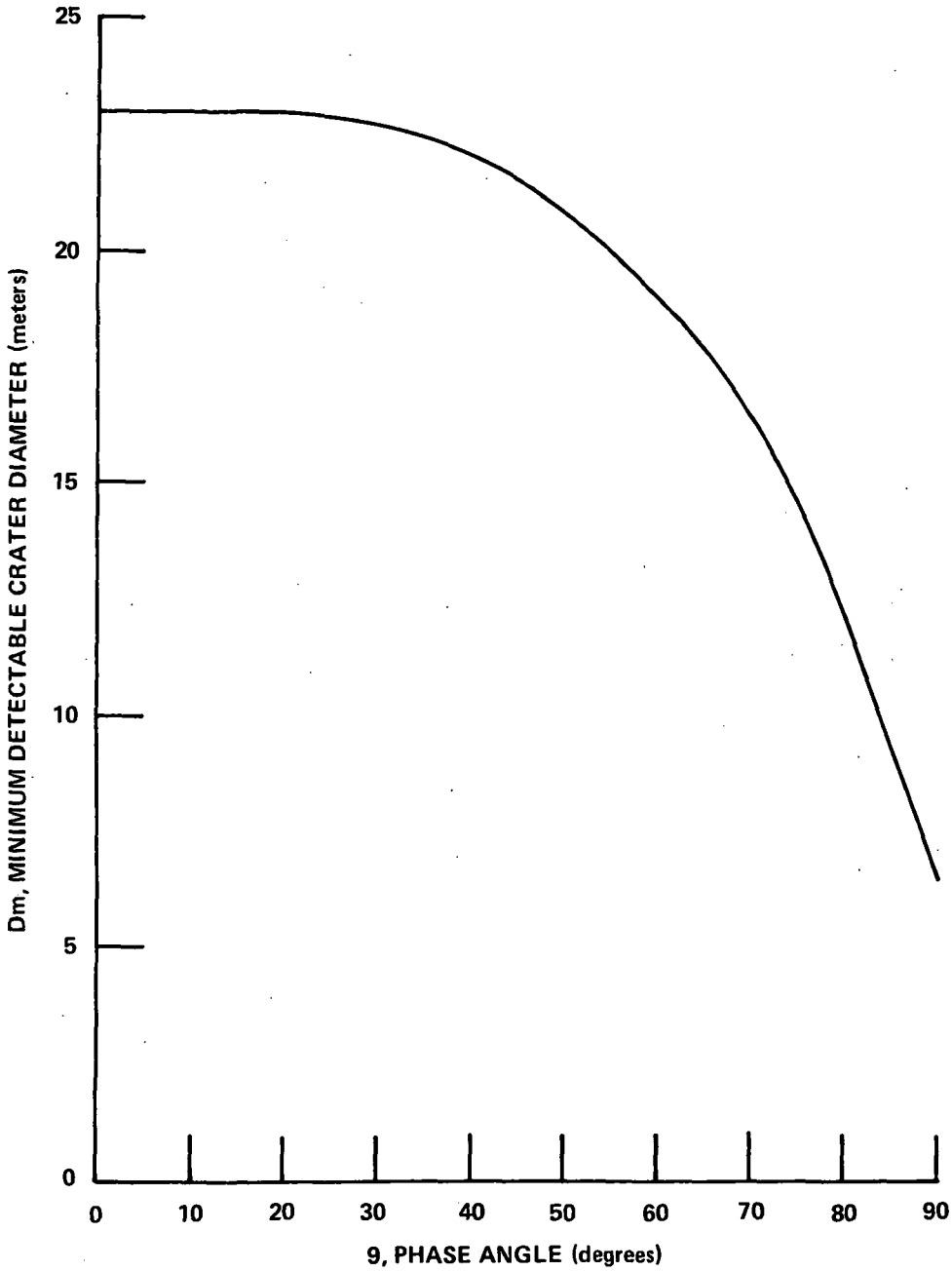

Figure 2 EFFECT OF PHASE ANGLE ON INFORMATION CONTENT OF NEAR VERTICAL LUNAR ORBITER PHOTOGRAPHY

resolution limit of the Mariner IX imagery is offset by the smaller phase angles at which the imagery was obtained. A comparison of TV and photographic imagery of the moon shows that image enhancement allows the TV image to approach the limiting resolution of 2.2 TV lines. However, the enhancement can distort topographic features which are on the order of several resolution elements.

Since the radiance of a point on a planetary surface depends upon the incident and emission angles measured with respect to the local surface normal, an accurate measure of surface radiance can be interpreted in terms of the surface orientation if the bidirectional reflectivity function for the surface is known. The conversion of surface radiance measured from an image into local slope and subsequently into a topographic profile has been termed "photoclinometry" and was applied to both Ranger (Rindfleisch, 1966) and Lunar Orbiter (Lambiotte, 1967) imagery. In the Lunar Orbiter application, the technique was used to derive relative surface roughness indices at potential Apollo landing sites. An evaluation of the quality of Lunar Orbiter imagery (Kinzly, 1968) showed that the medium resolution photographs of Missions I and II received excessive exposure and the image densities could not be reliably converted to surface radiance. The limitation that this placed on the application of photoclinometry was investigated (Gambell, 1968). More recently photoclinometry was used on Mariner IV imagery to produce depth/diameter data for martian craters (Cintala, 1976). Because of the nonlinear relationship between surface radiance and surface slope, the average radiance measured by an imaging system is not necessarily equivalent to the average slope of the surface -- both averaged over a resolution element. Consequently,

the resolution of the imaging system can affect the accuracy of the profile information generated by photoclinometry. This analytical procedure, to the best of our knowledge, has nevery received widespread application beyond Lunar Orbiter.

4.2 Definition of Global Geology

As noted in Section 3, differences in the normal albedo of a planetary surface can be produced by chemical or mineralogical differences, particle size differences or a combination of these effects. Consequently, a geologist frequently makes use of the normal albedo of the surface as an aid in defining geologic units. This potential utilization led to the development of albedo maps of the moon (Pohn, 1970), Mars (Cutts, 1971 and de Vaucouleurs, 1973) and Mercury (Dzurisin, 1976). In addition to the fact that albedo boundaries can be coincident with the boundaries between different geological units, correlation between reflectivity of surficial materials has been noted to vary inversely with age on the lunar surface -- older and more heavily cratered areas having a higher reflectivity.

In addition to the production of albedo maps which are used in qualitative geologic evaluations, analysis of the reflectivity characteristics of the light and dark areas of a planet on the global scale have been used to draw inferences on the composition of surficial materials. Typical examples of these type of analyses have included those of Pollack and Sagan (1967) where it was concluded that the bright and dark areas of Mars appeared to have a very similar chemical composition with goethite, a major constituent of both

areas. It was also suggested that both areas were covered by a fine powder and that the seasonal change in the reflectivity of the dark areas was produced by aeolian transport of material to and from the dark areas. The average diameter of the particles in the bright areas is estimated to be 50 μm while the dark areas were estimated to have particles ranging from 200 μm to 400 μm depending upon the period relative to the seasonal darkening. Based on visible polarimetry and IR radiometry they proposed limonite as a primary constituent of this powder.

A second example of global reflectivity analysis is that of Binder and Jones (1972). Observations were made using a ten channel spectroradiometer operating from 0.60 - 2.27 μm. They concluded that the measured spectro-reflectivity fell into two well-defined groups, mare and desert units, indicating that the martian surface consists of two types of materials. By comparison with laboratory data they proposed that both surface units contained lithic soils having a limonite stain and that the soils of the maria are richer in pyroxene, olivine, or both than the desert soils. This investigation, therefore, suggests that the differences between martian maria and deserts are due to composition and not due to differences in particle size as proposed by Pollack and Sagan.

A third example of global reflectivity investigations is the work of McCord and his associates (McCord and Adams, 1968; Adams and McCord, 1969; McCord and Westphal, 1971). These investigations involved spectroradiometric observation of Mars from 0.30 - 2.5 μm. Comparison of the resulting spectro-

reflectivity curves to laboratory data led to the conclusion that oxidized basalts are a significant constituent of the martian surface. Evidence has been suggested for the existence of basaltic flows and mare on Mars, thereby supporting this hypothesis. It should be noted, however, that the Mariner IX imagery acquired after a martian dust storm contained numerous bright and dark areas produced by dynamic aeolian transport of material over the martian surface. These observations support the hypothesis by Pollack and Sagan that the seasonal changes in reflectivity are a result of a change in the average particle size. It is, of course, quite possible that both mechanisms play a role in the dynamic characteristics of the reflectivity of the martian surface.

4.3 Interpretation of Local Reflectivity Differences

The evaluation of local changes in planetary surface reflectivity requires the availability of radiometrically calibrated high resolution imagery. Consequently, the techniques available for such analyses are less developed although they parallel those used in evaluation of reflectivity changes on a global scale. The distinction that we make between global and localized analyses can be correlated directly with earth-based versus spacecraft observations of the planet. An example of the qualitative analyses of local reflectivity variations is the use of the radial bright ray patterns associated with some craters on the lunar surface in order to derive relative ages. Quantitative techniques are available as illustrated in this report to analyze the dark and light markings occurring in the Mariner VI and VII imagery.

As noted in the previous section, Young and Collins (1971) analyzed the Mariner VI and VII far encounter photographs to derive the parameters of the Minnaert photometric function for five regions of the martian surface. We consider this analysis to be global rather than local, however, since it only employed the far encounter pictures which have resolutions ranging from 10 - 100 km.

A method for evaluation of local changes in the reflectivity of soils employing radiometric analysis using conventional color aerial photography has been recently reported (Piech, 1974). The technique was developed to assist in terrestrial soil surveys by supplementing conventional land form analyses with reflectivity information extracted from color imagery. The cause of reflectivity variations in a soil unit are evaluated by computing the ratio of the reflectance in two spectral bands. Information on the relative soil moisture and texture characteristics is derived from the reflectivity ratios obtained from the imagery. In this case the aerial camera is employed as a radiometer. In addition to calibration of the object-to-image radiometric response, the effects of the atmosphere must be removed from the imagery in the earth-based application. This is accomplished by radiometric analysis of standard scene objects such as shadow areas. If the darker soil element has a greater red-to-blue reflectivity ratio than the lighter soil element, the reflectivity variation is caused by differences in moisture content. If the darker soil element has a smaller ratio, the decrease in reflectivity is produced by an increase in the average particle size. Rather than computing the reflectivity ratios in two spectral bands the equivalent procedure of

computing the ratio of the reflectivity of the darker unit to the lighter unit in each of the spectral bands selected can be used. If the ratio of the darker to lighter soil element at the longer wavelength (e.g. red) is less than the ratio at a shorter wavelength (e.g. blue) then the change in reflectivity can be attributed to a larger particle size for the darker element. Figure 3 shows laboratory data obtained in support of this analysis technique. The figure shows the ratio of the darker to lighter (i.e. wet to dry) soil elements for several terrestrial sands and varying amounts of moisture content. The reflectivity ratios were obtained from densitometer measurements of vertical photography (normal emission) obtained under ambient sunlight such that the incident angle and phase angle varied from 30^{o} to 50^{o}. Note that the ratio increases with wavelength supporting the interpretation of reflectivity ratios proposed above. In the case of reflectivity changes due to particle size variation, the ratio decreases with increasing wavelength. Additional experimental data is presented in the cited reference. This size-reflectivity change rule is not applicable to all types of minerals that could be constituents of soils. The reflectivity versus size effect has been investigated for likely martian surface materials (Salisbury, 1968) and is discussed further in Section 5.2.

The application of this analysis technique to adjacent light and dark surficial elements on the martian surface can be used to distinguish between a chemical cause for lower reflectivity, namely absorbed moisture or a physical cause due to varying particle size. Note that if the composition

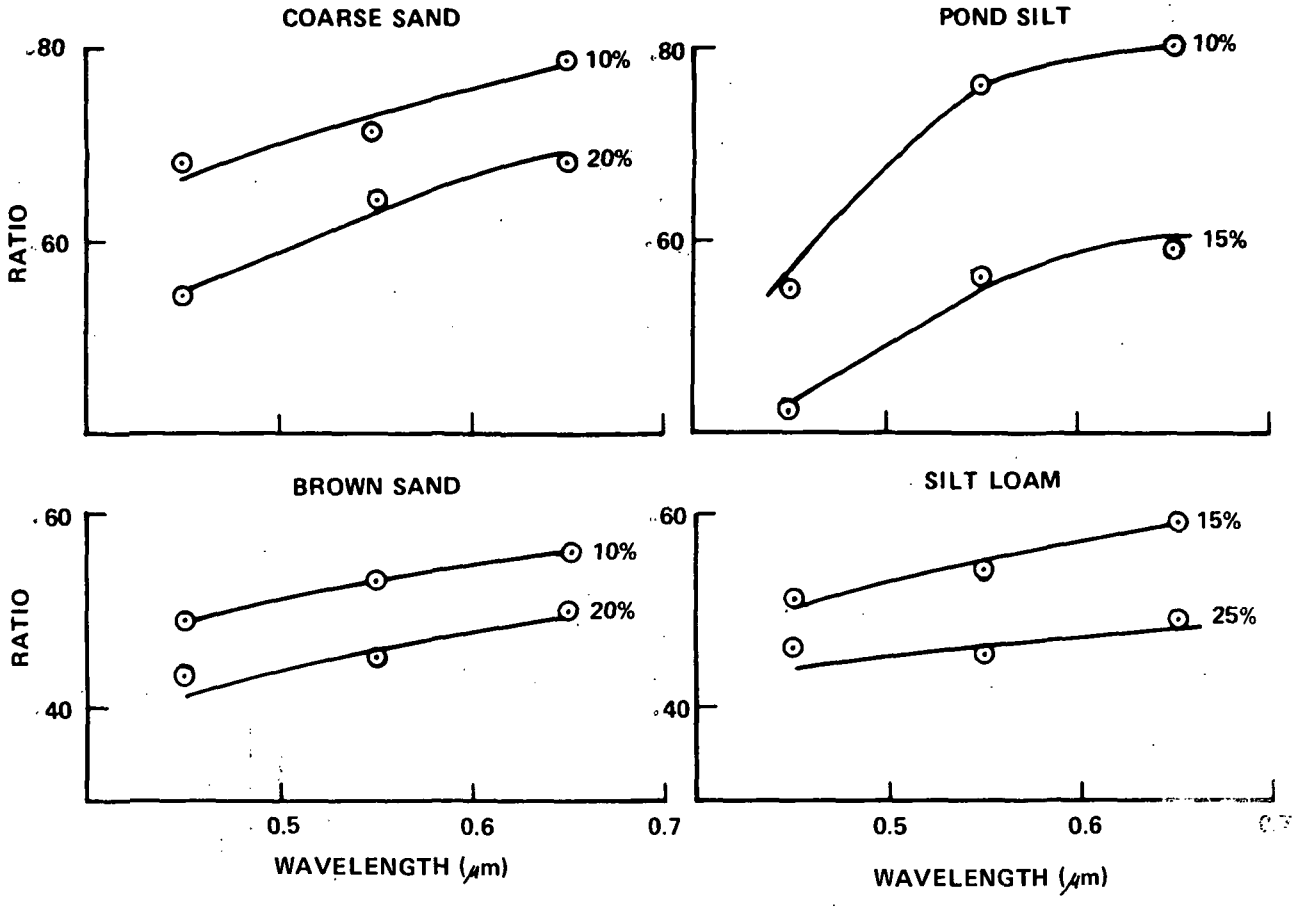

Figure 3 WET/DRY RATIOS DETERMINED PHOTOGRAPHICALLY FOR VARIOUS TERRESTRIAL SOILS AND MOISTURE CONTENTS BY WEIGHT

of the light and dark areas is assumed to be similar or if the bidirectional reflectivity is assumed constant, the ratio of the radiance of the dark to the light area is equal to the ratio of their reflectivities and no explicit correction for the bidirectional reflectivity or photometric function is required. This technique was applied to the analysis of adjacent light and dark areas occurring in the Mariner VI and VII imagery -- the results are presented in the next section of this report.

SECTION 5

ANALYSIS OF MARINER VI AND VII IMAGERY

This section of our report documents analyses carried out on Mariner VI and VII imagery to interpret local variations in reflectivity by using reflectivity ratios derived from the imagery. Darkening of the martian surficial material can be produced by chemical effects such as absorbed water, by changes in the particle size or by changes in the composition of the surface material. Identification of the presence of significant amounts of moisture in the martian soil is important to the assessment of life forms on Mars while the assessment of relative particle size differences is important to the evaluation of dynamic aeolian processes. Alternate near encounter frames from the wide angle Mariner cameras were taken through different spectral filters (red, green or blue) and the overlap between successive frames show the same area of the martian surface in two spectral bands. These regions of overlap provide an opportunity to use reflectivity ratio analysis techniques in the study of martian planetology. In this section we (1) identify the areas where bi-band spectral data is available, (2) present additional data in support of the interpretation of the reflectivity ratios beyond that identified previously in Section 4.3, (3) describe the tools developed to compute the reflectivity ratios from digital data supplied by the Image Processing Laboratory at JPL and (4) present the results of the analysis of adjacent light and dark areas occurring in the Mariner photography.

5.1 Mariner VI and VII Multi-Spectral Image Data

The objective of this investigation was to illustrate the utility of radiometric analysis, particularly reflectivity ratios, to planetology in general and the study of Mars in particular. We planned to use TV image data obtained from the Mariner VI, VII and IX missions. Mariner VI and VII were fly-by missions that had a variety of experiments including a dual TV imaging system (Danielson, 1971). One TV sensor employed a short focal length lens ($\sim$50mm) while the second sensor employed a long focal length lens ($\sim$500mm) and were termed the "wide angle" and "narrow angle" cameras respectively. Since the imagery was obtained during fly-bys the resolution ($\sim$2.2 TV lines) changed from image to image. For the imagery utilized it was approximately 2-4 km for Mariner VI and 4-5 km for Mariner VII. The wide angle camera contained a filter wheel with four spectral filters. The spectral transmission of the filters incorporated into Mariner VI and VII are shown in Figure 4. Alternate near encounter frames from the wide angle Mariner cameras overlapped such that the same area of the martian surface was taken through two different spectral filters. The initial step in the research effort was the identification of those areas where bi-band coverage was available. Reflectivity ratios computed within these areas could be used for geologic mapping, discrimination of atmospheric phenomena, obtaining information about polar cap structure and obtaining information about the cause of local variations in the reflectivity of the martian surficial material.

Six areas of bi-band coverage were identified from the Mariner VI mission and six areas of bi-band coverage from the Mariner VII mission.

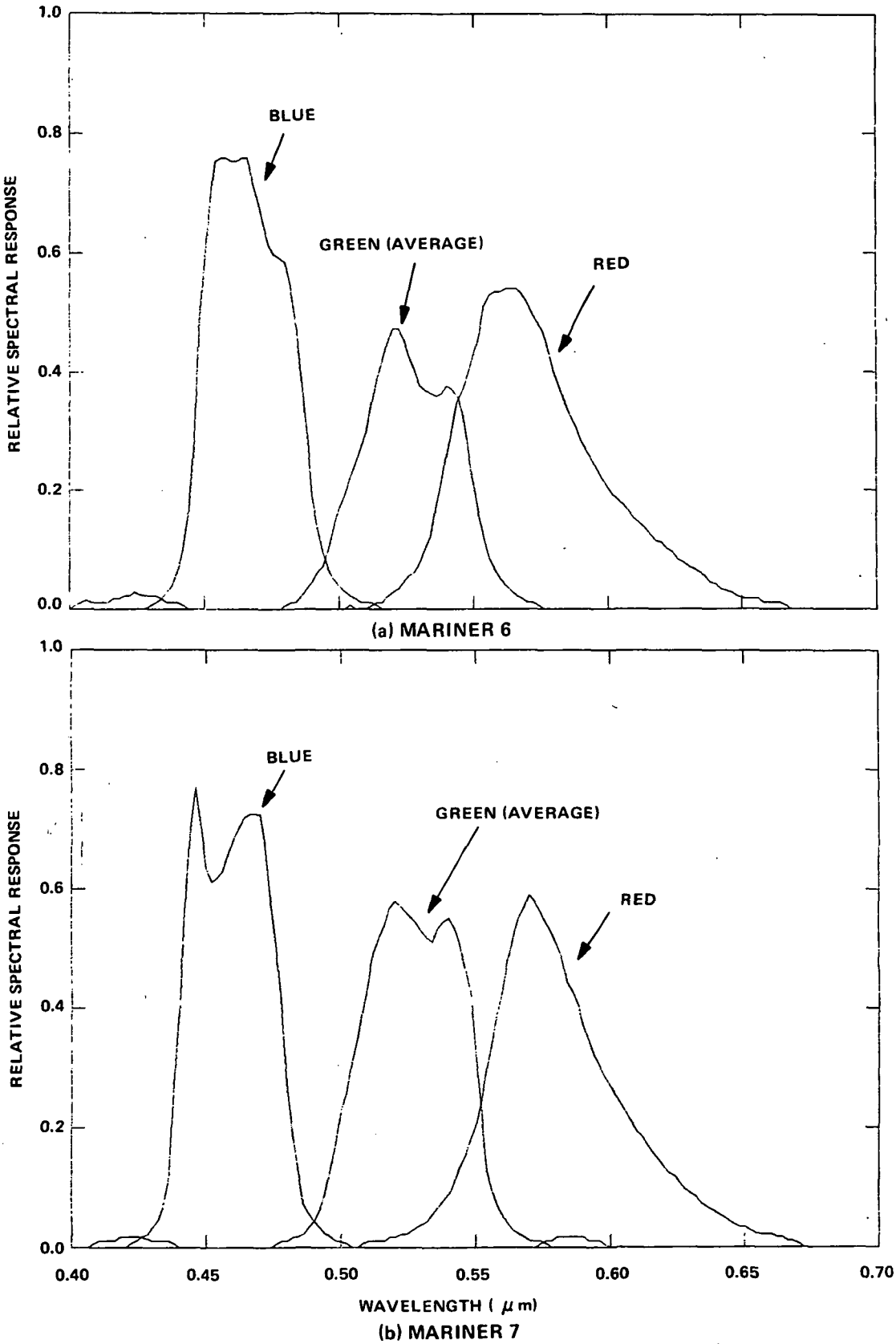

Figure 4 SPECTRAL TRANSMISSION OF MARINER VI AND VII WIDE ANGLE CAMERAS

Table 3 summarizes these areas which are designated by the mission number followed by a letter code A through G. This table identifies the location of each of these areas and the frame numbers and spectral filters of each of the overlapping photographs. Figure 5 shows the location of each of the bi-band coverage areas on the 1971 Shaded Relief Map of Mars.

A number of potential bi-band coverage areas were eliminated from consideration. These included the two areas of overlap between 7N5, 7N7 and 7N9. These photographs were obtained at a highly oblique angle and had lower resolution than the subsequent near encounter frames. Consequently the radiometrically corrected digital imagery was not requested from JPL. In retrospect this is somewhat unfortunate since these photographs included some of the areas in Meridiani Sinus coincident with areas 6B and 6C previously selected. In addition, the overlap area between frames 7N29 and 7N31 were deleted from consideration because of their proximity to the terminator which yields a lower quality due to the low exposure level on the vidicon. One area of overlapping coverage among frames 7N15, 7N17 and 7N19 actually had tri-band coverage. This is a small area in the South Polar Cap located at 72°S - 80°S, 332°W - 348°W. Although no specific analysis was undertaken over this area, several features appear that might be caused by atmospheric phemonena. Figures 6 through 9 show the Mariner VI bi-band coverage areas on enhanced versions of the imagery transformed to othographic projections. Figures 10 through 13 show the bi-band coverage areas of Mariner VII on similar projections. Digital tapes containing TV image data for each frame identified in Table 3 were obtained from Mr. A. Collins at the

Table 3a

Mariner Bi-band Coverage Areas
Mariner VI

DESIG-NATION	REGION	LOCATION	FRAME NO.	SPECTRAL BANDS	OVERLAP (APPROX.)	PHASE ANGLE	GEOLOGIC UNIT*	PRINCIPAL MAPPING QUADRANGLE(S)
6A	Aurorae Sinus - Margaritifer Sinus	2°N - 19°S, 28°W - 47°W	6N5, 6N7	Red,Green 1	40%	51°	cu, h	Margaritifer Sinus
6B	Thymiamata	11°N - 13°S, 2°W - 15°W	6N9, 6N11	Blue,Green 2	40%	51°	cu	Oxia Palus - Margaritifer Sinus
6C	North Meridiani Sinus & West Edom	7°N - 10°S 352°W - 30°W	6N11, 6N13	Green 2,Red	30%	51°	cu	Sabaeus Sinus
6D	Margaritifer Sinus and East	9°S - 23°S, 13°W - 23°W	6N15, 6N17	Green 1,Blue	25%	80°	cu	Margaritifer Sinus
6E	Margaritifer Sinus and East	13°S - 21°S, 1°W - 6°W	6N17, 6N19	Blue,Green 2	25%	80°	cu	Margaritifer Sinus
6F	Sabaeus Sinus and West	12°S - 21°S, 350°W -353°W	6N19, 6N21	Green 2,Red	25%	80°	cu	Sabaeus Sinus
6G	Sabaeus Sinus and West	11°S - 20°S 338°W -341°W	6N21, 6N23	Red,Green 1	25%	80°	cu	Sabaeus Sinus

*List of Units (after Carr, 1973)

h: Chaotic Deposits
cu: Cratered Deposits, Undivided

Table 3b

Mariner Bi-band Coverage Areas
Mariner VII

DESIG-NATION	REGION	LOCATION	FRAME NO.	SPECTRAL BANDS	OVERLAP (APPROX.)	PHASE ANGLE	GEOLOGIC UNIT*	PRINCIPAL MAPPING QUADRANGLE(S)
7A	Edge Polar Cap	50°S - 70°S, 2°W - 56°W	7N11, 7N13	Green 2,Red	50°	35°	cm,cu,ps	Argyre
7B	Polar Cap	57°S - 79°S, 342°W - 56°W	7N13, 7N15	Green 2,Red	50°	35°	cm,cu	Argyre - Mare Australe
7C	Polar Cap	64°S - 86°S 322°W - 26°W	7N15, 7N17	Red,Green 1	50°	35°	?	Mare Australe
7D	Polar Cap	68°S - 88°S 292°W - 4°W	7N17, 7N19	Green 1,Blue	50°	35°	?	Mare Australe
7E	Noachis - Hellas	29°S - 44°S 322°W -342°W	7N23, 7N25	Green 1,Blue	25%	80°	cu	Noachis
7F	Boundary Helle-spontus Hellas Boundary	38°S - 48°S 311°W -322°W	7N25, 7N27	Blue,Green 2	15%	80°	cu,m,ps	Noachis - Hellas
7G	Hellas Floor	40°S - 45°S 295°W -303°W	7N27, 7N29	Green 2,Red	small	80°	ps	Hellas

*List of Units (after Carr, 1973)

cm: Cratered Deposits, Mantled
cu: Cratered Deposits, Undivided
ps: Sparsely Cratered Plains
m: Mountainous Deposits

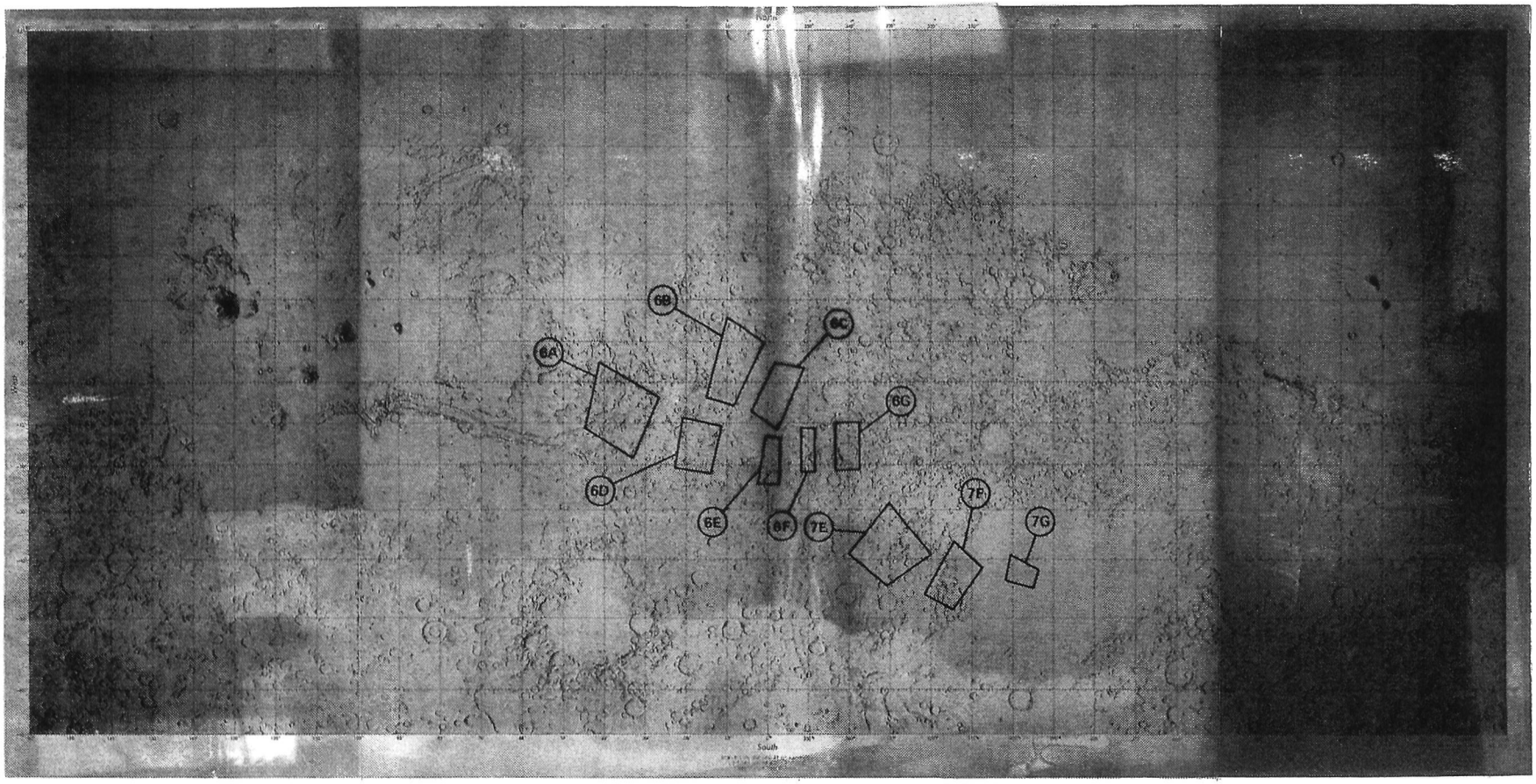

Figure 5 BI-BAND COVERAGE AREAS ON MARS

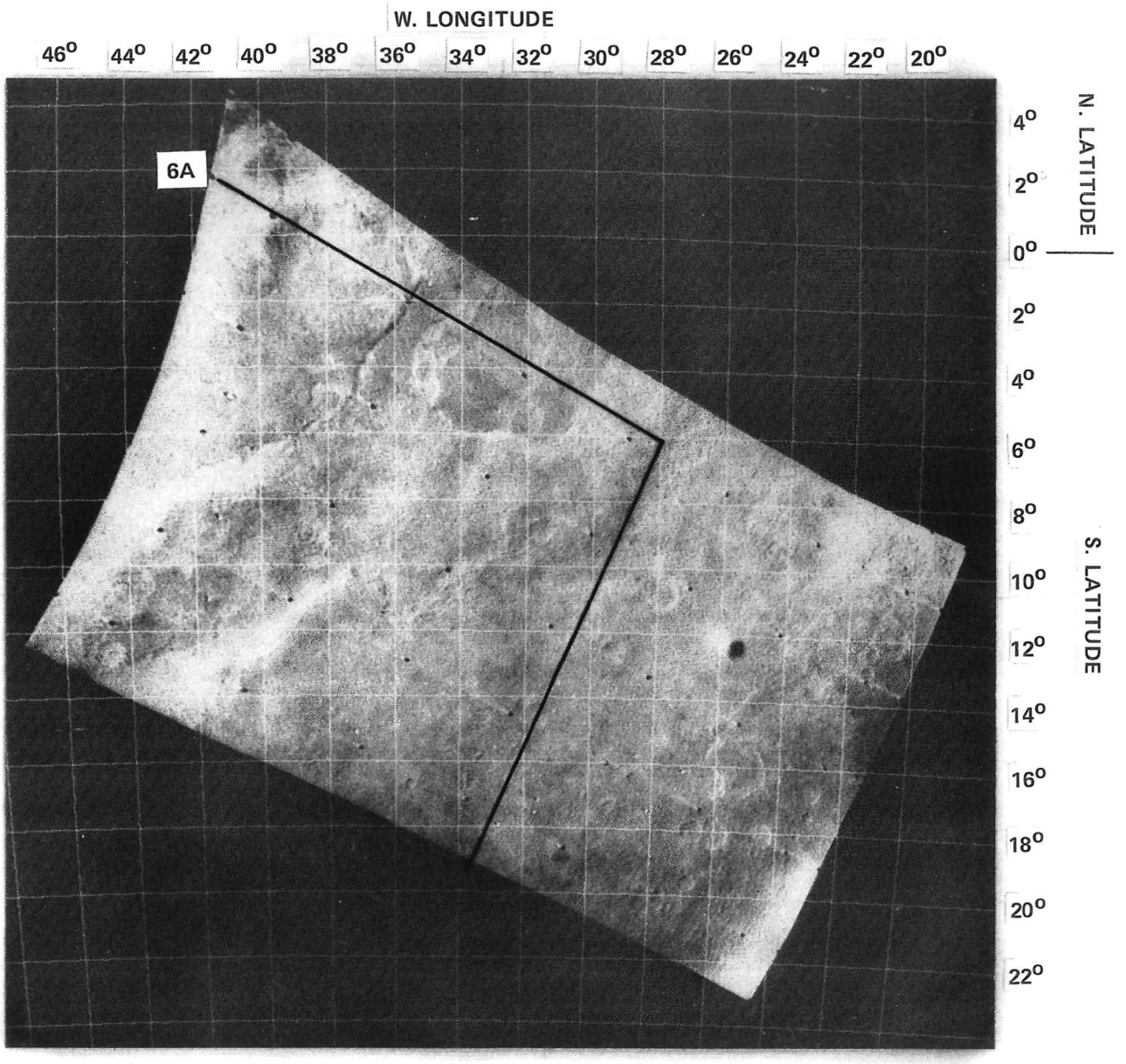

Figure 6 BI-BAND AREA 6A SHOWN ON ORTHOGRAPHIC PROJECTION OF FRAME 6N7

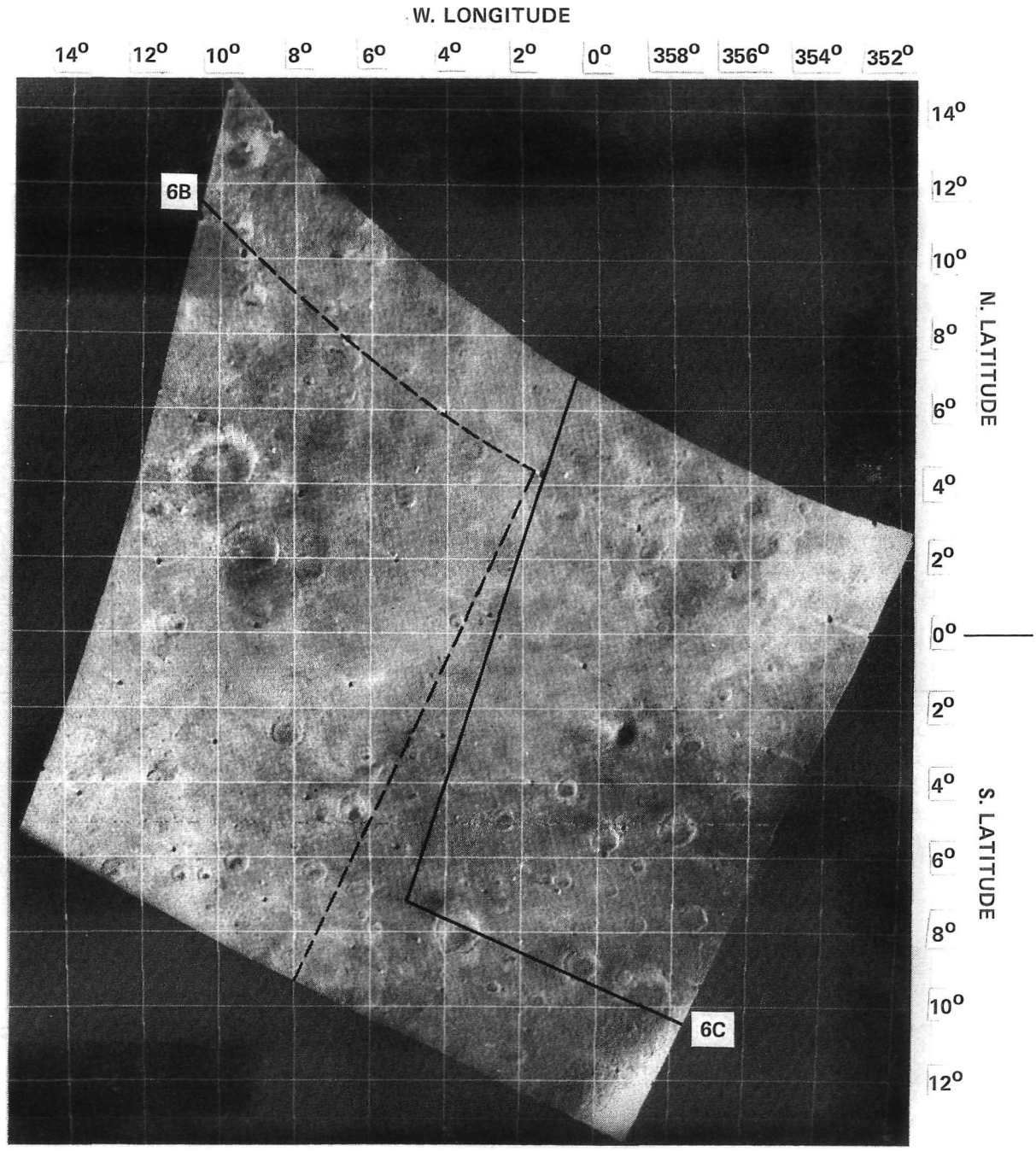

Figure 7 BI-BAND AREAS 6B AND 6C SHOWN ON ORTHOGRAPHIC PROJECTION OF FRAME 6N11

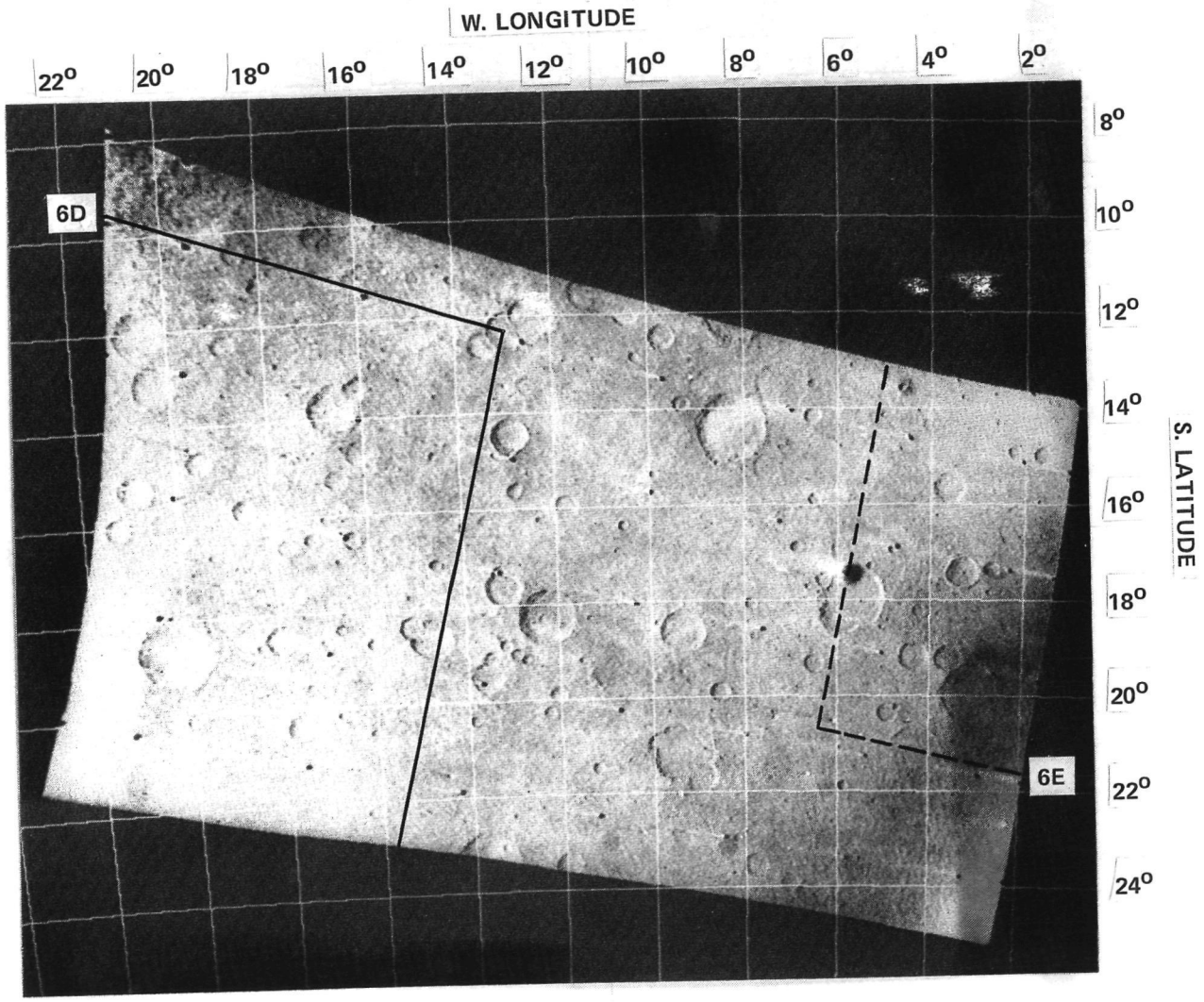

Figure 8 BI-BAND AREAS 6D AND 6E SHOWN ON ORTHOGRAPHIC PROJECTION OF FRAME 6N17

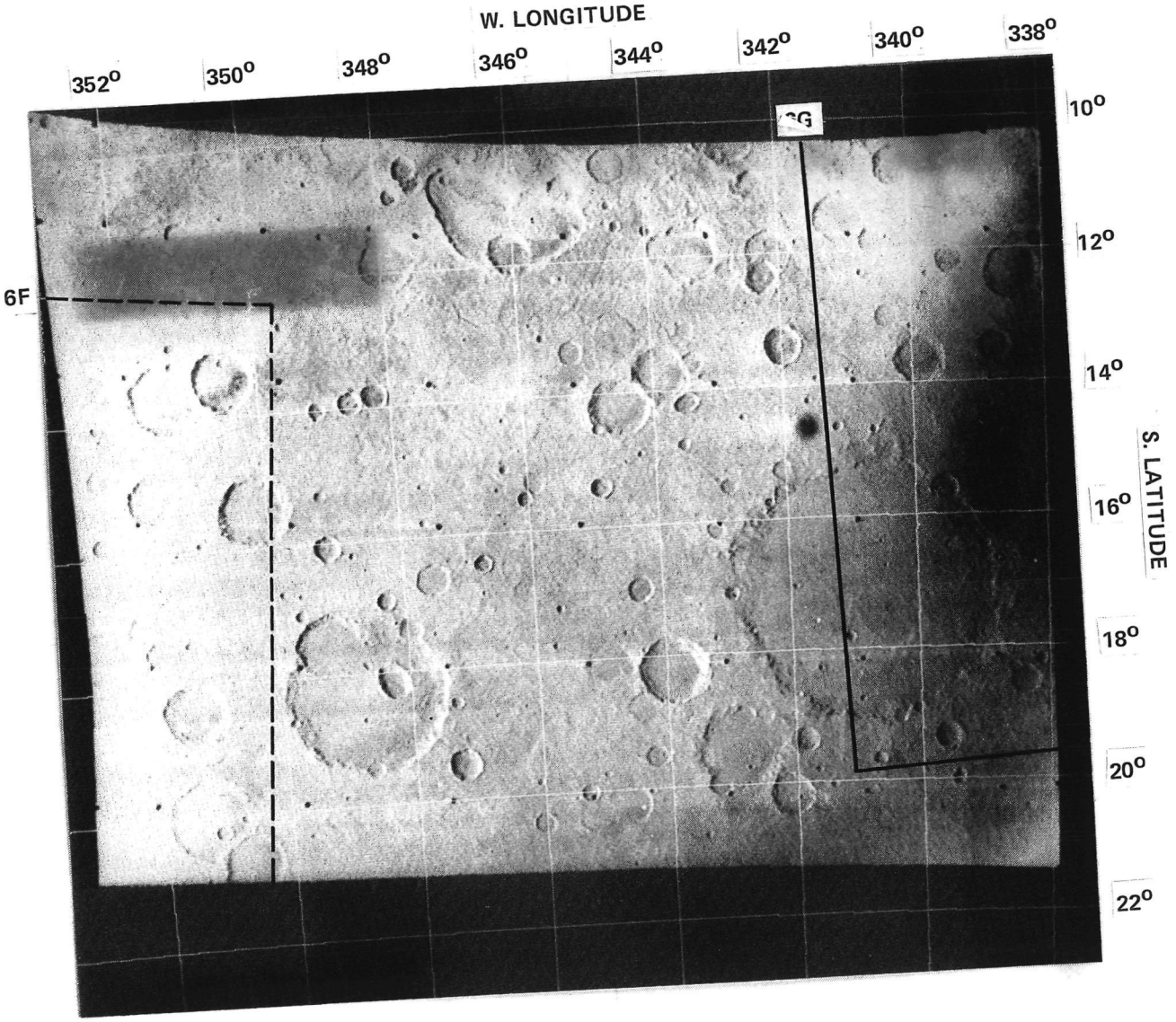

Figure 9 BI-BAND AREA 6F AND 6G SHOWN ON ORTHOGRAPHIC PROJECTION OF FRAME 6N21

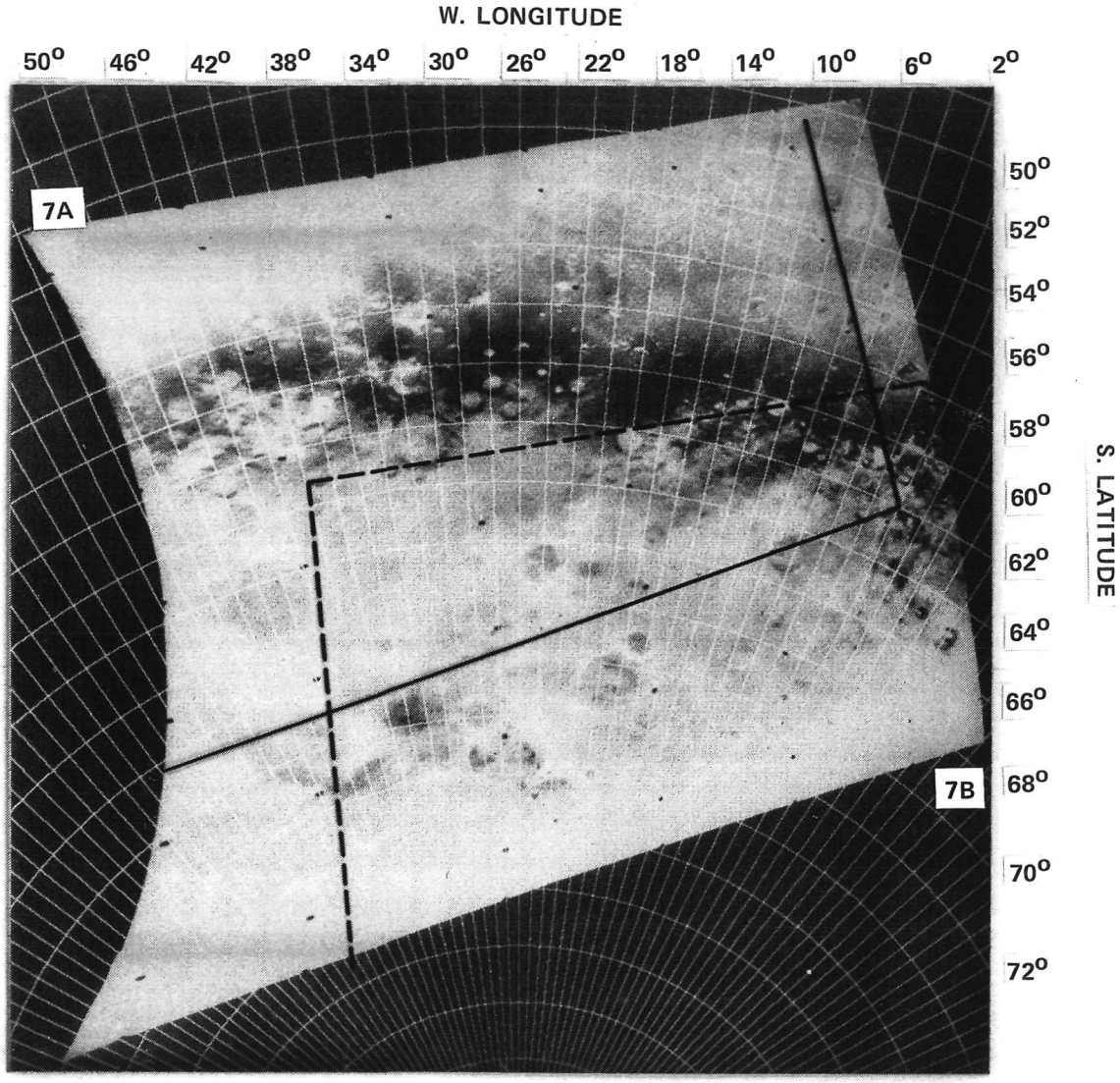

Figure 10 BI-BAND AREAS 7A AND 7B SHOWN ON ORTHOGRAPHIC PROJECTION OF FRAME 7N13

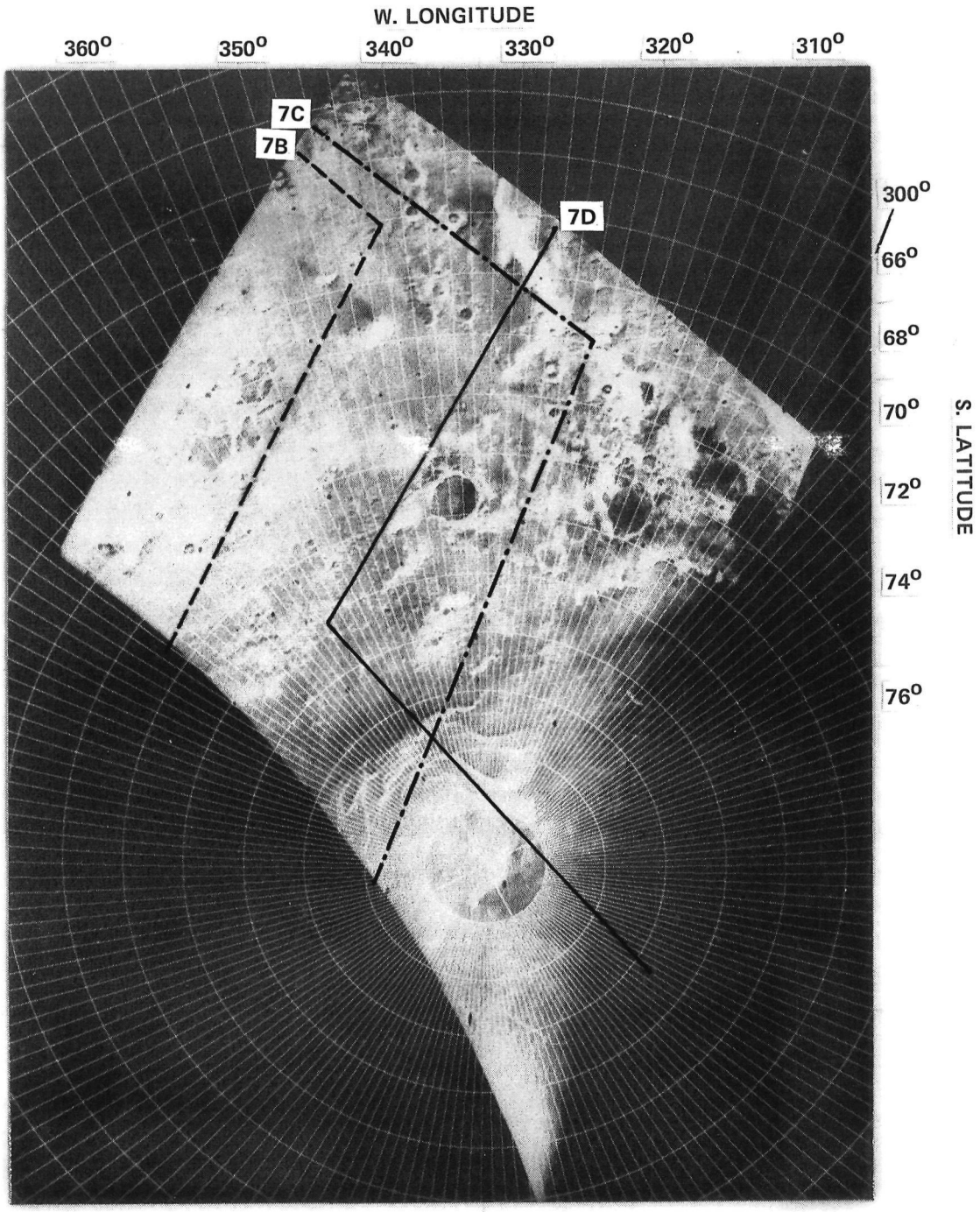

Figure 11 BI-BAND AREAS 7B, 7C AND 7D SHOWN ON ORTHOGRAPHIC PROJECTION OF FRAME 7N17

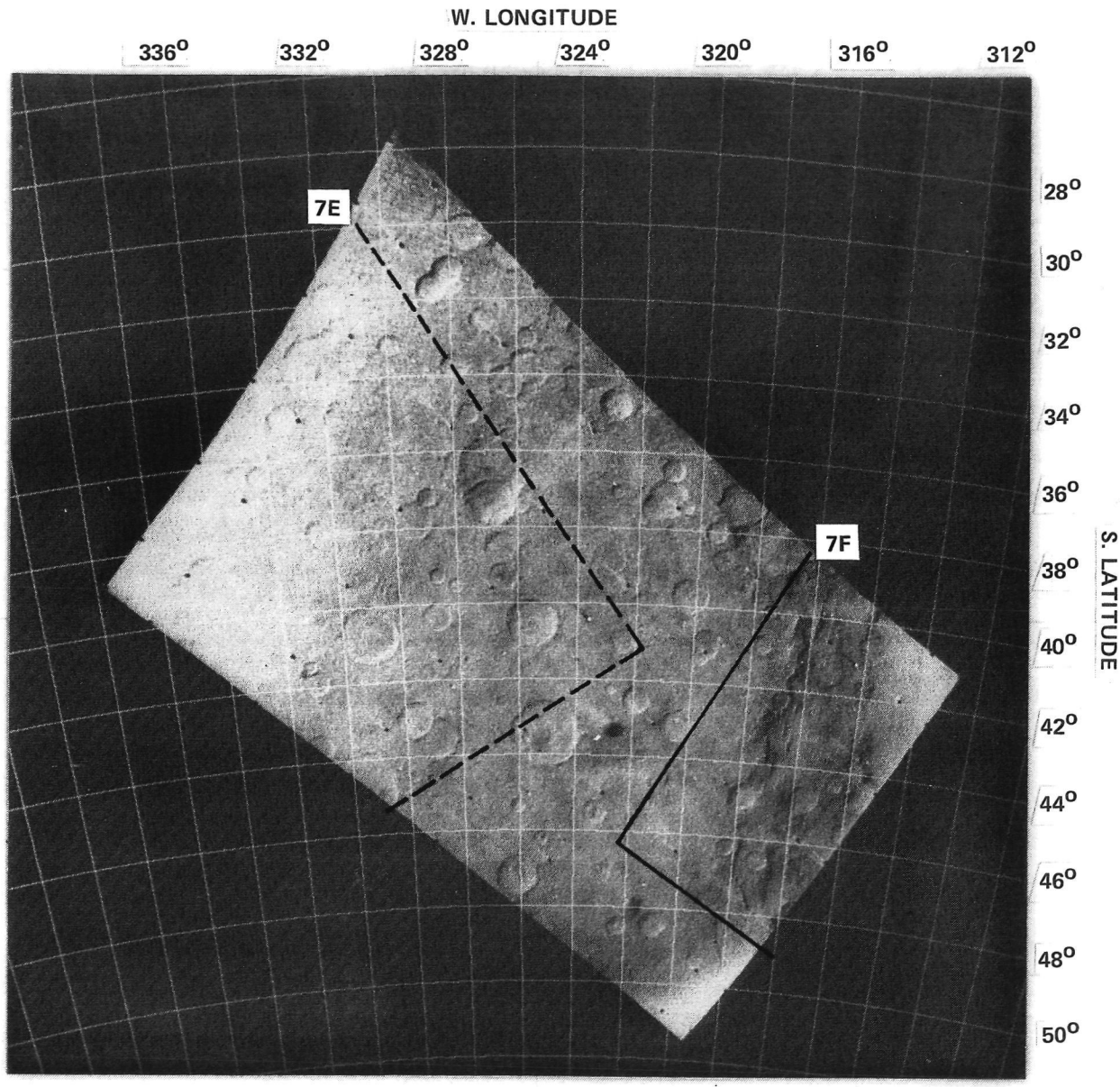

Figure 12 BI-BAND AREAS 7E AND 7F SHOWN ON ORTHOGRAPHIC PROJECTION OF FRAME 7N25

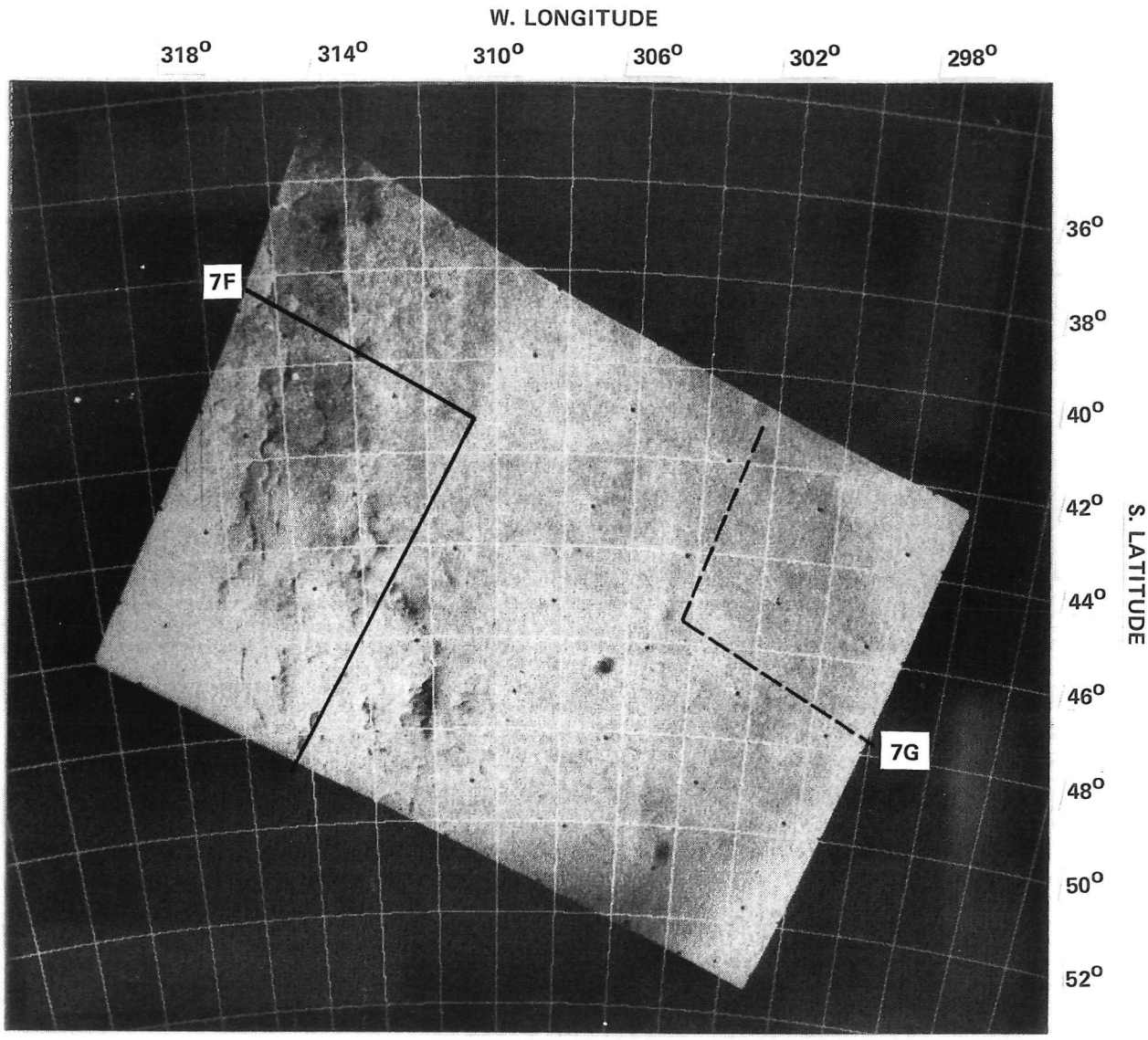

Figure 13 BI-BAND AREAS 7F AND 7G SHOWN ON ORTHOGRAPHIC PROJECTION OF FRAME 7N27

Jet Propulsion Laboratory. The data obtained was the LMICOR version which was produced by the Image Processing Laboratory at JPL by correcting the raw TV data for radiometric distortion introduced by the TV systems. The corrected data represents the surface bidirectional reflectivity multiplied by a factor of 6.0 in order to optimally utilize an 8-bit format.

The area that received the most detailed analysis was 6C. This area has light and dark markings on crater floors which were evaluated to determine whether this variation is caused by absorbed water or by changes in particle size. The method employed uses the reflectivity ratios in the manner discussed in Section 4.3. Section 5.2 contains additional data on the relationship between particle size and reflectivity that supports our analysis of these markings. The results of the analysis itself are contained in Section 5.4.

5.2 Reflectivity - Particle Size Effect

A size-reflectivity change rule was described in Section 4.3 that has been utilized in terrestrial soil surveys. This rule indicated that the reflectivity ratio of the dark-to-light soil element should decrease with increasing wavelength if a change in particle size was responsible for the change in reflectivity.

The proposal that limonite be a major constituent of the martian surface led Salisbury and Hunt (1968) to conduct a study of the spectral behavior of likely martian surface materials. They classified potential

materials by their change in reflectivity as a function of particle size. The class of transparent materials, which includes silicate minerals, show a increase in reflectivity with a decrease in particle size as assumed in the development of the size-reflectivity change rule referenced above. Opaque material, particularly metal sulfides, showing a decrease in reflectivity with decreasing particle size. A third class of materials which Salisbury and Hunt term "trans-opaque" exhibits a decrease in reflectivity in the opaque portion of the visible spectrum and an increase in reflectivity in the transparent portion of their visible spectrum. That is, the spectral reflectivity curve for one particle size will cross that for a different particle size leading to a reversal in reflectivity between the two particle sizes within the visible spectrum. This behavior is exhibited by several ferric oxides such as limonite, goethite and hematite that are likely candidates for existence on the martian surface. As Salisbury and Hunt point out, light and dark markings on the martian surface composed of high concentrations of these types of materials should exhibit a contrast reversal at some point in the visual spectral region. That is, the light markings should become dark and the dark markings become light as the radiometric or image data increase in wavelength. Since such a reversal has not been observed Salisbury and Hunt concluded that the hypothesis that the martian soil consists in a large part of limonite and that the reflectivity differences are due to particle size changes are incompatible. As an alternative they propose that the most likely soil is one composed of silicates lightly stained or coated with ferric oxides. In terms of the present evaluation of the Mariner imagery the dark-to-light reflectivity ratio could increase with

wavelength between the blue and green images and subsequently decrease with wavelength between the green and red images if a significant amount of the trans-opaque type materials composed the elements under evaluation and the change in particle size was the principal cause for the change in reflectivity. Our analysis concentrated on the local reflectivity changes occurring in bi-band coverage area 6C involving overlapping green and red imagery.

To further support our analyses using the reflectivity ratio, the ratios for typical martian materials were evaluated over the spectral responses of the Mariner VI and Mariner VII wide angle cameras presented earlier in Figure 4. Hunt and Salisbury (1970, 1971) have obtained a number of spectral reflectivity curves for various rocks and minerals as part of a laboratory study of spectroscopic remote sensing techniques. We selected typical candidates from the published data for silicate minerals (1970) and oxides and hydroxides (1971). The spectral reflectivity for each of the minerals selected is shown in Figure 14 (although measurements were made at IR wavelengths this data was not of interest here). The reflectivity data were obtained near normal incidence and emission angles at a phase angle of 15° and referenced to a Lambertian surface with a diffuse reflectivity near 1.0. Generally the data were obtained for four different particle size regions allowing six different ratios of the reflectivity of larger-to-smaller particle sizes to be obtained. For materials whose reflectivity increases with decreasing particle size this ratio is equivalent to that of the darker-to-lighter soil elements. The six different ratios obtained are identified in Table 4 using the letter symbol A through F.

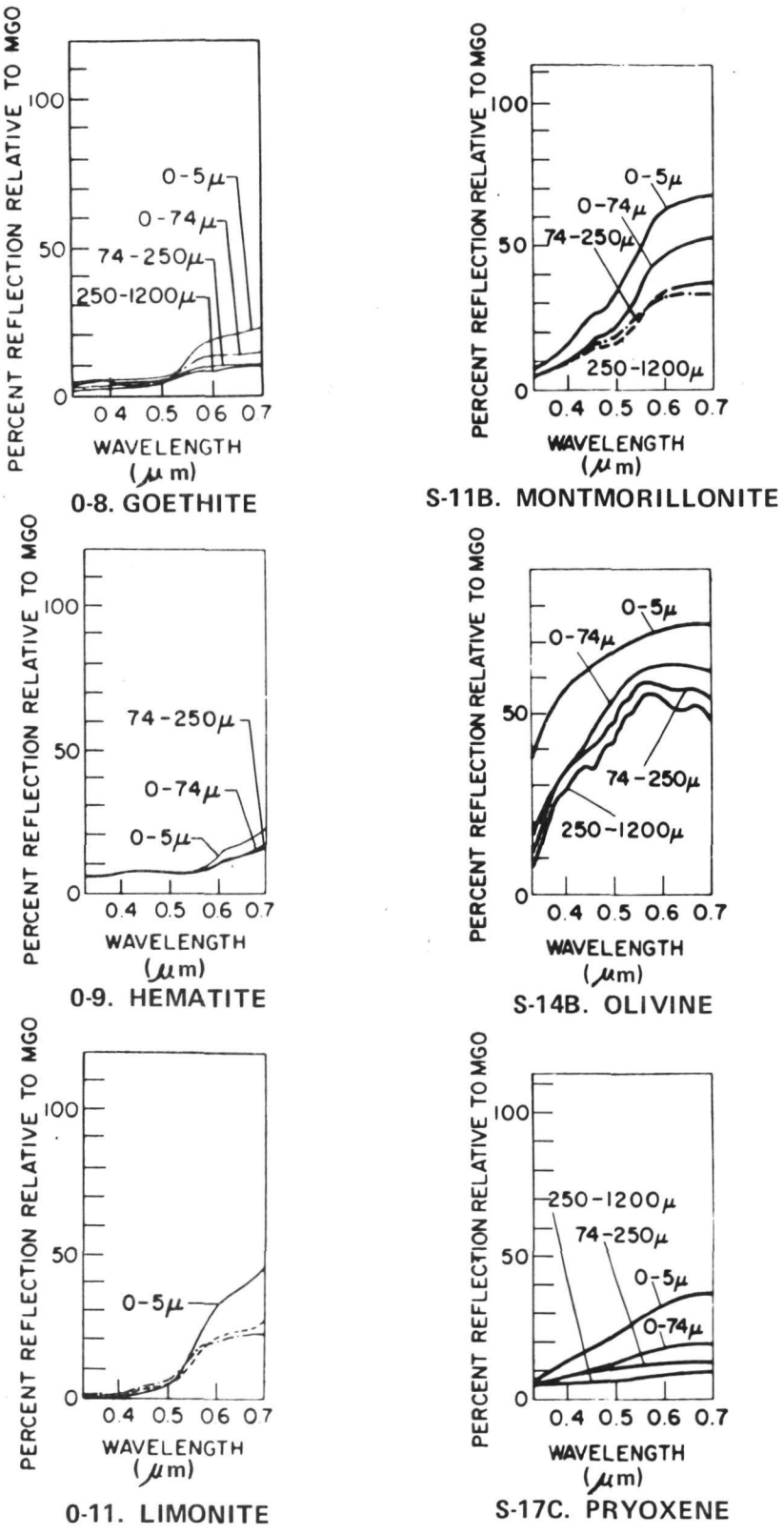

Figure 14 SPECTRAL REFLECTIVITY FOR TYPICAL MARTIAN MINERALS AS A FUNCTION OF PARTICLE SIZE

Table 4

Large-to-Small Particle Index

Symbol	Particle Size Ratio
A	250-1200 μm/0-5 μm
B	250-1200 μm/0-74 μm
C	250-1200 μm/74-250 μm
D	74-250 μm/0-5 μm
E	74-250 μm/0-74 μm
F	0-74 μm/0-5 μm

From the silicate minerals olivine and pyroxene were selected based upon the analysis of Binder and Jones (1972). Montmorillonite was arbitrarily added as the third selection from the silicate minerals. Limonite was selected from the ferric oxides since it has been proposed as a major constituent by Pollack and Sagan (1967) and as a stain on silicates by Binder and Jones (1972) and Salisbury and Hunt (1968). Pollack and Sagan proposed goethite as a major constituent of the martian surface and consequently this was also selected by the oxide group. Finally, Hematite was added as a third ferric oxide--a logical addition to those already selected. Table 5 presents the average reflectivity of these minerals within the Mariner VI and VII spectral bands. As the table shows, the reflectivity increases with decreasing particle size in all cases except for the smallest particle size group of goethite in the green band (and presumably the blue band) and for all of the particle size groups measured in the case of limonite for both the blue and green spectral bands. Consequently, the ratio of the larger-to-smaller particle size groups obtained from this data are equivalent to the ratio of the darker-to-lighter surface elements except for the cases cited.

Table 5

Average Reflectivity of Potential
Martian Materials Within the Mariner Spectral Bands

Mineral	Size Range	Mariner VI			Mariner VII		
		Blue	Green	Red	Blue	Green	Red
0-8 Goethite	250-1200 μm	.048	.064	.083	.049	.064	.085
	74- 250 μm	.039	.065	.089	.037	.066	.092
	0- 74 μm	.060	.080	.116	.059	.081	.121
	0- 5 μm	?	.078	.152	?	.079	.162
0-9 Hematite	74- 250 μm	.072	.068	.082	.072	.068	.087
	0- 74 μm	.080	.075	.089	.081	.075	.093
	0- 5 μm	.081	.080	.103	.081	.080	.110
0-11 Limonite	250-1200 μm	.054	.104	.174	.053	.106	.182
	0- 74 μm	.040	.088	.164	.040	.089	.177
	0- 5 μm	.030	.097	.228	.029	.099	.250
S-11B Mont-morillonite	250-1200 μm	.144	.201	.292	.143	.203	.306
	74- 250 μm	.166	.227	.290	.162	.229	.298
	0- 74 μm	.186	.276	.404	.182	.279	.422
	0- 5 μm	.270	.407	.547	.265	.411	.568
S-14B Olivine	250-1200 μm	.373	.478	.536	.365	.481	.539
	74- 250 μm	.427	.530	.577	.418	.533	.578
	0- 74 μm	.473	.573	.617	.459	.576	.620
	0- 5 μm	.637	.681	.713	.631	.682	.718
S-17C Pyroxene	250-1200 μm	.058	.066	.077	.057	.066	.079
	74- 250 μm	.098	.113	.120	.096	.114	.121
	0- 74 μm	.108	.137	.162	.105	.138	.165
	0- 5 μm	.193	.254	.305	.188	.256	.312

Figure 15 shows the reflectivity ratios determined for the ferric oxide samples and the Mariner VI spectral response functions. The ratios were plotted at the effective focal length for each of the spectral filters as specified by Danielson (1971). Figure 16 is the corresponding plot for the silicate samples. The results obtained in the case of Mariner VII are similar to the reflectivity ratios shown here. We would expect that the ratios would approach unity as the particle size differences between the two groups being ratioed decreases. In addition, the rate of change of the ratio with respect to wavelength should decrease as the particle size differences decrease, i.e., the slope of the curve becomes less. If we compare the progression of curves for cases A to B to C we would expect that these phenomena would be apparent in Figures 15 and 16. Except for the cases where a reversal in the change of reflectivity with particle size occurs, this phenomena is exhibited for all of the minerals evaluated. A similar trend is exhibited in going from the curves with index D to the curves of index E. We can infer from these results that information about the relative difference in particle sizes can be obtained by examining the level and slope of the reflectivity ratio versus wavelength curve. The difference between the ratio from the green to the red band is presented in Table 6. In this table a positive number indicates a decrease in the ratio as the wavelength is increased as expected from the size-reflectivity change rule stated previously. Note that most of the changes are positive (i.e., show a decrease with increasing wavelength) except for olivine which shows an increase in the ratio for all cases. If we eliminate this sample from consideration the average value of the change which is also presented in the table is greatest for the A ratio which has

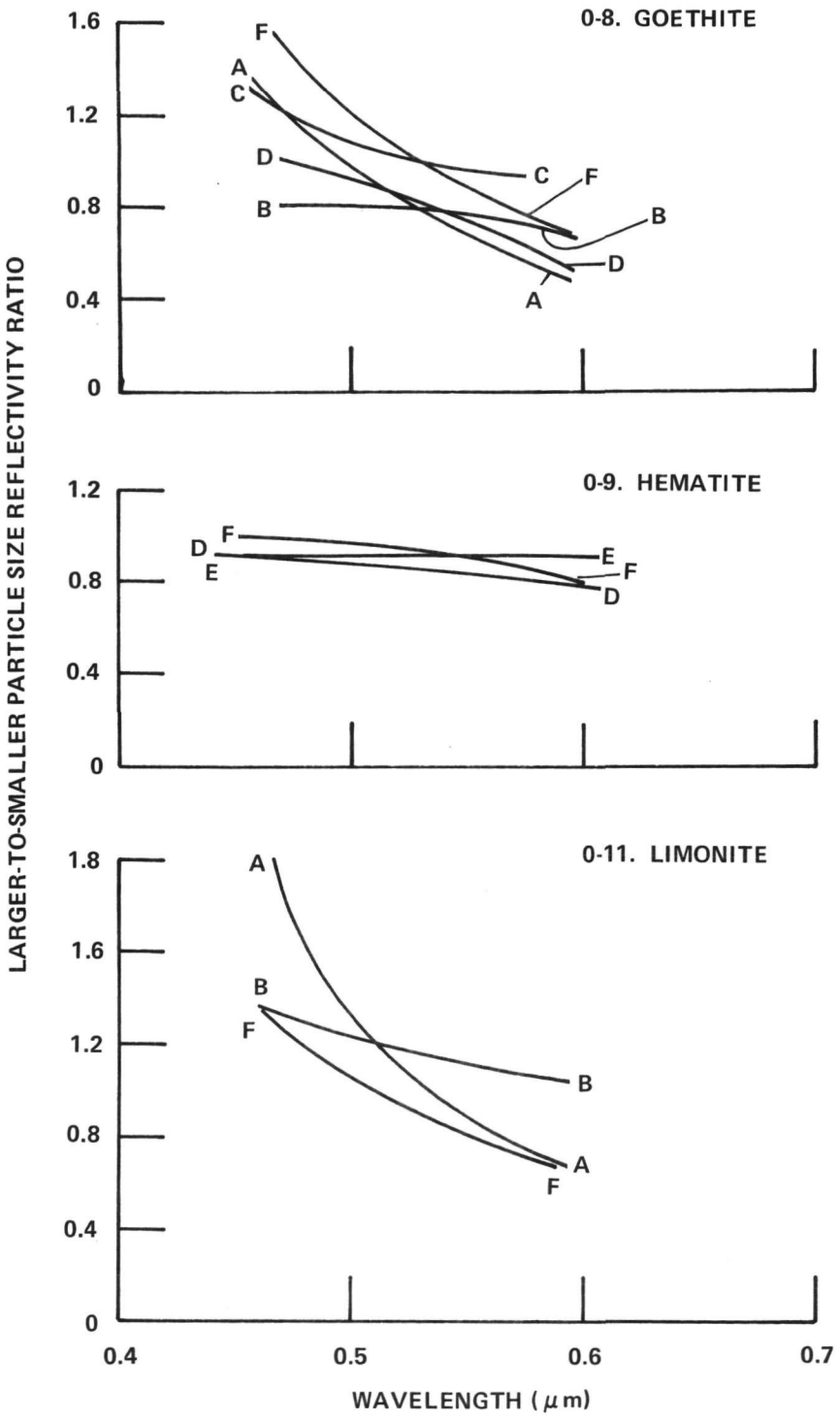

Figure 15 REFLECTIVITY RATIOS FOR SELECTED OXIDES AND VARIOUS PARTICLE SIZE GROUPS

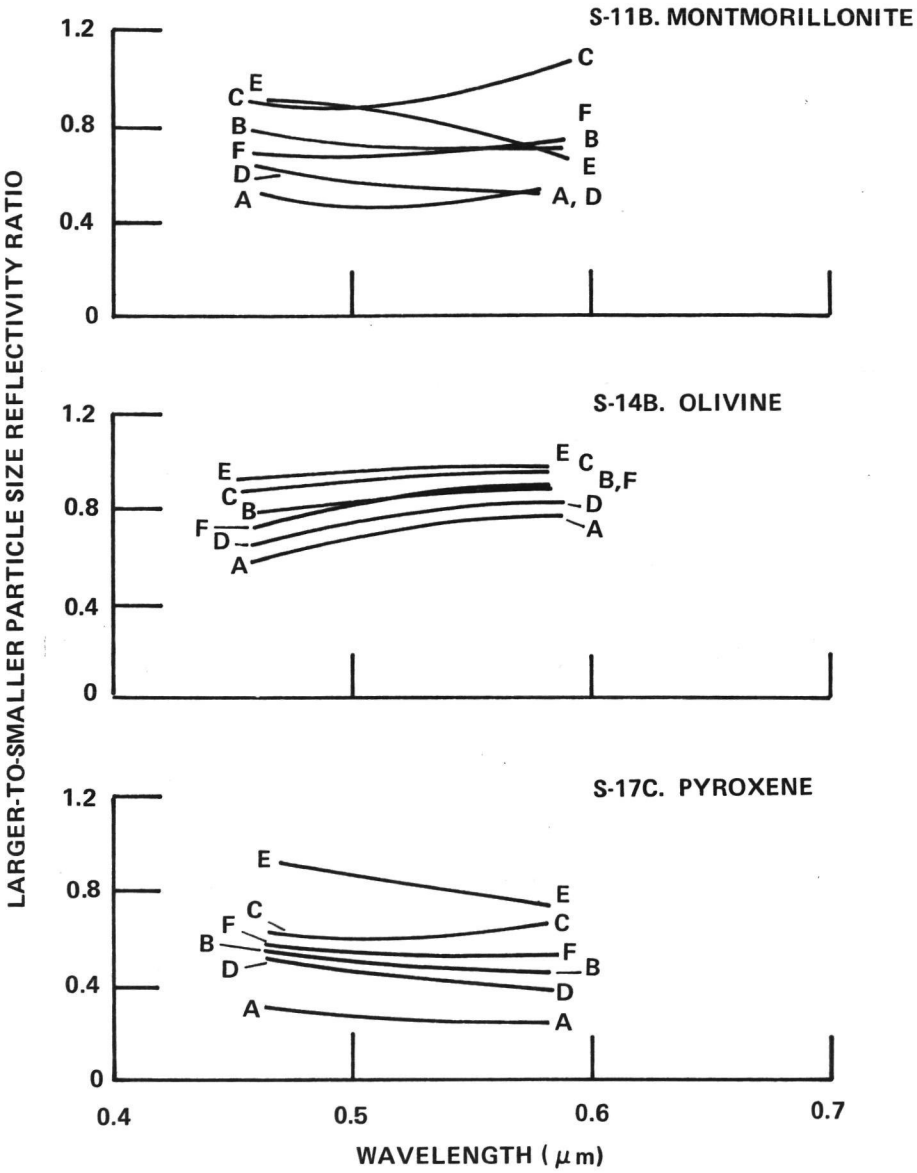

Figure 16 REFLECTIVITY RATIOS FOR SELECTED SILICATES AND VARIOUS PARTICLE SIZE GROUPS

Table 6

Green-to-Red Decrease in the Reflectivity Ratio

Index	0-8 Goethite	0-9 Hematite	0-11 Limonite	S-11B Montmorillonite	S-14B Olivine	S-17C Pyroxene	Average (w/o Olivine)
A	.27	-	.31	-.04	-.03	.01	.14
B	.08	-	.12	.01	-.04	.00	.05
C	.05	-	-	-.11	-.05	-.06	-.04
D	.24	.05	-	.03	-.02	.05	.09
E	.04	-.01	-	.10	-.03	.08	.05
F	.30	.08	.19	-.06	-.03	.01	.10

the largest particle size differences and least (negative) for the C ratio where the particle size differences are not as great. Consequently, we conclude that the slope of the reflectivity ratio versus wavelength curve indeed does contain information about the relative particle size of the materials producing the light and dark markings.

5.3 Evaluation of the Light and Dark Markings Associated with Craters

Bi-band coverage area 6C contained several craters with light and dark markings located interior to the crater on their floor. Several of these craters were chosen for subsequent analysis of the reflectivity ratio of these markings from frames 6N11 and 6N13. The craters selected are shown in Figure 17. The light and dark markings were located by sample and line number and subsequently retrieved from the LMICOR images contained on digital tape supplied by JPL. Software programs were developed to retrieve this data over a rectangular area specified by the initial and final sample and line number. A description of this software is presented in the appendix to this report. Table 7 contains the average reflectivity and subsequent ratio for each of the selected dark and light markings in the red and green spectral bands.

These data are not the only source of reflectivity ratios of dark-to-light markings on the martina surface. Dollfus measured the dark-to-light area contrasts in several wavelength bands. These data were employed by Pollack and Sagan (1967) and were extracted for comparison to our results. These results are presented in Table 8. Other studies utilizing reflectivity

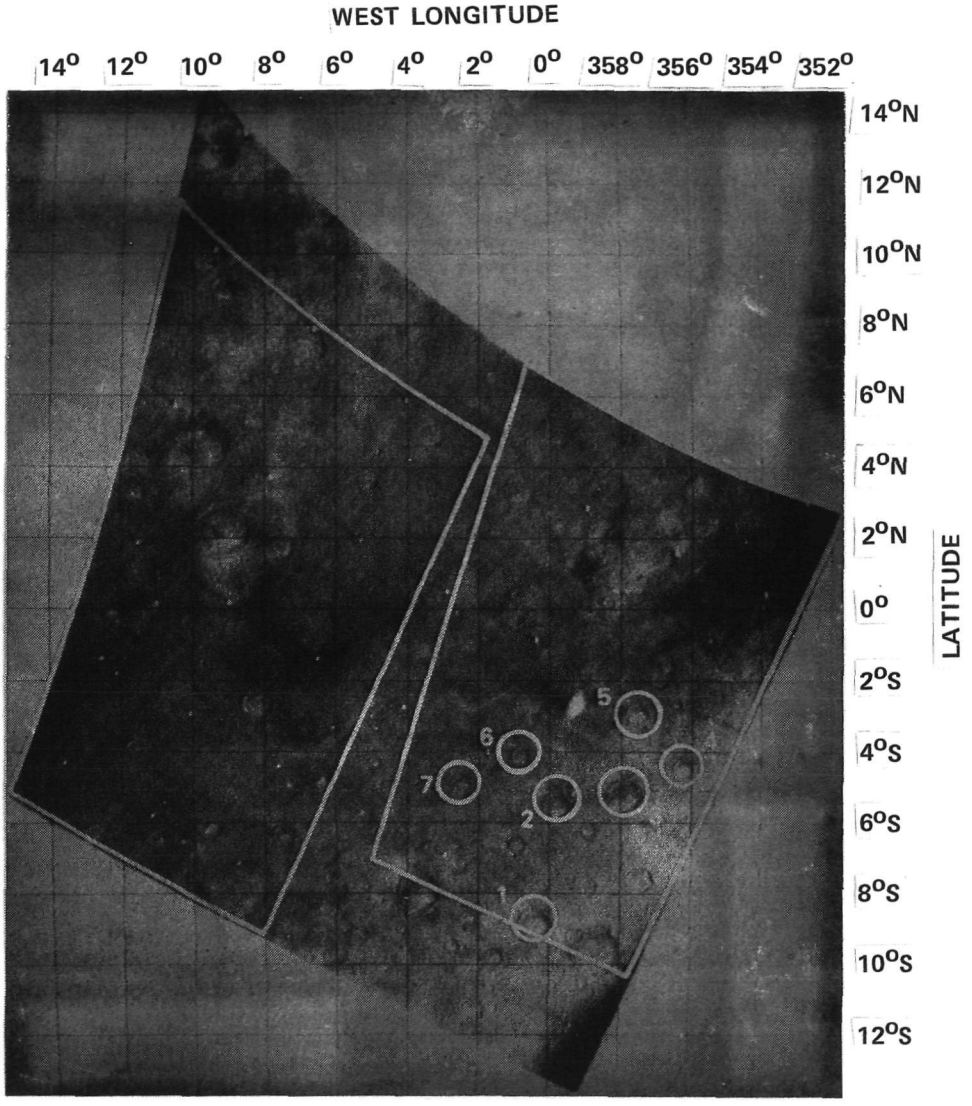

Figure 17 CRATERS ANALYZED IN BI-BAND COVERAGE AREA 6C

Table 7

Reflectivity and Reflectivity Ratio of Crater Markings

Target	6N11-Green (.53 μm)			6N13-Red (.58 μm)		
	Dark	Light	Ratio	Dark	Light	Ratio
1 - Crater	.0588	.0602	.977	.0742	.0879	.844
2 - Crater	.0583	.0633	.921	.0708	.0843	.840
3 - Crater	.0592	.0640	.925	.0658	.0816	.806
4 - Crater	.0604	.0632	.956	.0668	.0754	.886
5 - Crater	.0598	.0641	.933	.0665	.0767	.867
6 - Crater	.0603	.0651	.926	.0717	.0806	.890
7 - Crater	.0599	.0638	.939	.0734	.0764	.961
Average	.0595	.0634	.940	.0699	.0804	.871
σ	.0009	.0015	.020	.0035	.0046	.049

Δ = Green-to-Red Change = .07

Table 8

Normal Reflectivity and Dark-to-Light Reflectivity Ratios Derived from Dollfus Contrast Data

λ (μm)	Dark Areas	Bright Areas	Ratio
.45	.065	.071	.92
.50	.098	.120	.82
.55	.120	.164	.73
.60	.139	.210	.66
.65	.150	.250	.60

Δ = Effective Green-to-Red Change = .09

ratios were conducted by McCord (1969) and by Cutts (1971). McCord studied selected dark and bright regions primarily the Arabia-Syrtus Major pair at 21 narrow spectral passbands in the visible spectrum. From his results, McCord concluded that the bright regions are much redder than the dark regions, that is the ratio of the reflectivity of the dark-to-light regions in the red region is greater than the blue region. According to the size-reflectivity change rule, this would indicate that particle size effects are probably responsible for the differences between the bright and dark martian regions. Cutts subsequently employed the McCord data to augment his evaluation which was obtained using the late far encounter images obtained during the Mariner VII mission. Cutts evaluated nine different regional areas ranging from high to low reflectivity. The reflectivity ratio for dark-to-light areas for selected data presented by Cutts is contained in Table 9. The first three ratios were selected to represent that of the darkest-to-lightest features. The second two ratios were selected because they represent moderately dark-to-light features. Note that the value of the reflectivity ratio is closer to one for the second group than the first group and that the change or average slope of the reflectivity ratio curve is less for the second group compared to the first group. The third group contains two cases, the first being the ratio between two relatively dark features and the second being the ratio between two relatively light features. Note in this case that the reflectivity ratios are much closer to unity and that the average slope is less than either of the two preceeding groups.

Table 9

Dark-to-Light Reflectivity Ratios Derived from
Selected Cutts/McCord Data Within Mariner Spectral Bands

	Description	Blue (.47μm)	Green (.53μm)	Red (.58μm)	(Green-to-Red)
I	Syrtis Major/Arabia*	.87	.77	.65	.12
	Margaritifer Sinus/Moab	.83	.73	.59	.14
	Meridiani Sinus/Moab	.84	.75	.65	.10
II	Deucalionis Regio/Moab	.97	.95	.93	.02
	Thymiamata/Moab	.92	.87	.80	.07
III	Meridiani Sinus/Sabaeus Sinus	.95	.94	.90	.04
	Edom/Moab	1.01	1.00	.97	.03

*After Cutts

All three data sources were plotted for comparison to the Mariner VI crater markings in Figures 18 and 19. Figure 18 shows that the crater markings show a change in ratio which indicates that particle size differences are responsible for the change in reflectivity (the ratio decreases with increasing wavelength). Furthermore, comparison of the Mariner results to that of Cutts and McCord indicates that the Mariner ratios represent more moderate changes in particle size than that due to the extreme reflectivity changes. The change in reflectivity ratio from green-to-red of 0.07 is compatible with those in Group II in Table 9 and is consistent with the changes obtained in Section 4.2 for particle size groups B and E. A similar result is exhibited in Figure 19 when compared with the Dollfus ratios. The Dollfus results appear to represent a larger change in reflectivity than that due to the crater markings. The

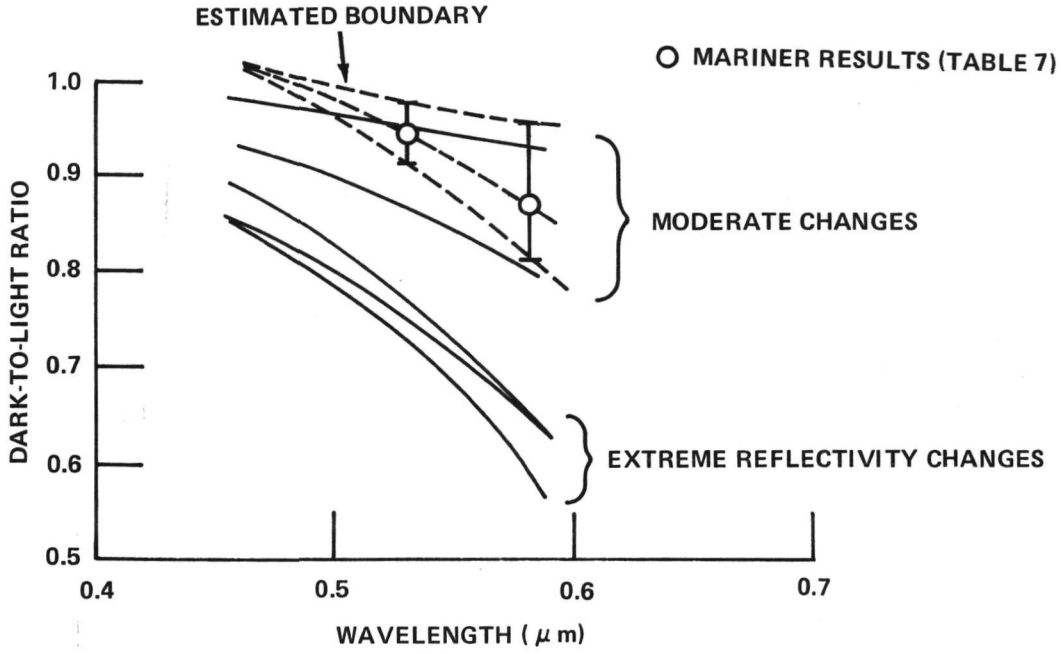

Figure 18 COMPARISON OF MARINER REFLECTIVITY RATIOS TO THOSE OF CUTTS AND McCORD

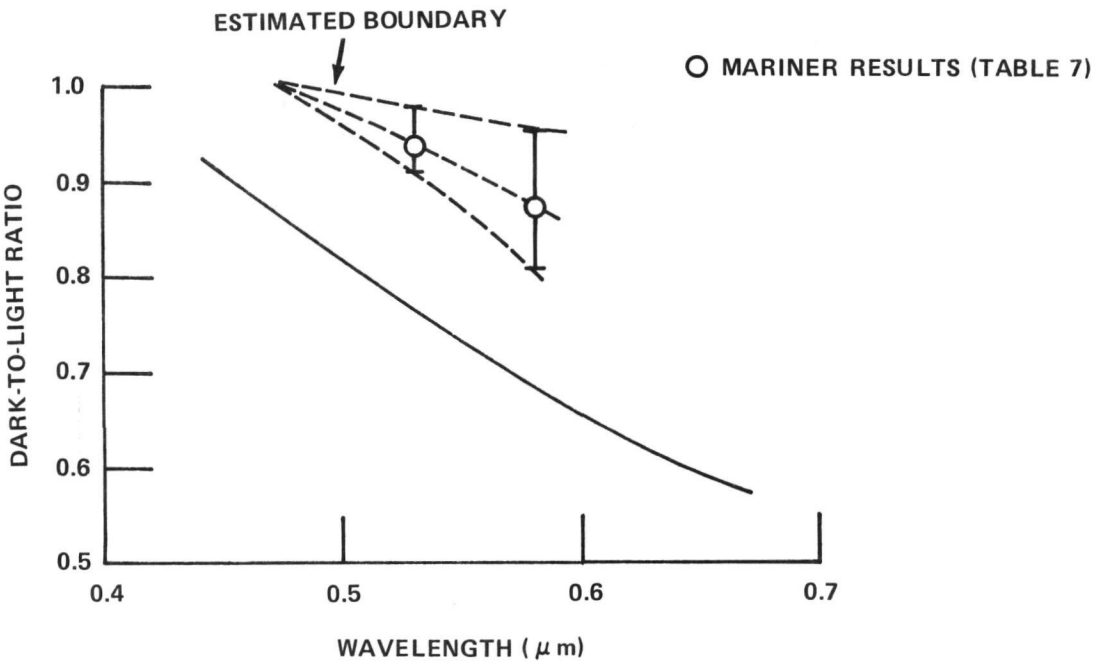

Figure 19 COMPARISON OF MARINER RATIO TO THOSE OF DOLLFUS

Group I data of Cutts and McCord (Table 9) and that of Dollfus (Table 8) are consistent with size Groups A and D in Section 4.2. Note that the size ranges represented by Groups B and E are compatible with the postulated mean particle sizes for the light and dark areas offered by Pollack and Sagan (1967).

If we compare the reflectivity presented in Table 5 to an extrapolation of the Minnaert parameter N_g obtained by Thorpe (Table 2) we find that the normal reflectivity of olivine appears to be a factor of 2-3 greater than the average normal albedo. Consequently, limonite stained olivine is not considered to be a likely candidate as a major constituent on this local area. Limonite stained pyroxene appears to be the best candidate based upon the data obtained during the course of this effort. Of course this conclusion must be somewhat tenuous since a number of mineral compositions could yield the results obtained.

5.4 Mariner IX Imagery and Other Related Data

We had hoped to continue the present effort using Mariner IX image data obtained through multiple spectral filters. It was anticipated that a large number of multi-spectral coverages would be available. Unfortunately, the filter wheel mechanism became inoperative during Revolution 118 and only a very limited amount of multi-spectral data was obtained. For the subsequent portion of the Mariner mission image data was obtained using the orange polarizing filter contained in the fifth filter wheel position. During the initial part of the mission the martian surface was obscured by a dust storm and consequently no useful image data of surface features were obtained in

this part of the mission when the filter wheel was operative. Mariner IX did confirm that dynamic aeolian processes play a significant role in the reflectivity variations on the martian surface and that a significant number of these variations are caused by changes in particle size.

An analysis of the light and dark markings present in the Mariner IX imagery obtained subsequent to the subsiding of the dust storm was made by Arvidson (1974). As a result of his analysis he found that "dark splotched craters in regions with bright streaks usually have upwind bright patches, suggesting that these features formed by dumping of bright dust over crater rims ... ". This characteristic pattern minus the bright streaks downwind of the craters are identical to those that we have analyzed. Furthermore, they have a North to South orientation consistent with the direction of the wind pattern observed subsequent to the dust storm through analysis of the wind-blown streaks. In addition, a sequence of wind tunnel experiments have been carried out by Greeley and his associates (1974). The results of these experiments have generated light and dark markings similar to those observed during our effort and have further demonstrated that some of the dark markings occur from wind erosion and that some of the light markings are depositional in nature. The reader is also referred to a comparison of Mariner VI and VII imagery and Mariner IX imagery which includes the bi-band coverage area we analyzed for a qualitative assessment of effect of the dust storm on local reflectivity variations (Ververka, 1974).

Though it was intended to demonstrate the use of reflectivity ratios as an aid to geologic mapping, the lack of availability of Mariner IX imagery greatly degraded this objective. The Mariner VI and VII imagery within the bi-band coverage areas occurred over a limited number of geologic units and the detailed geologic maps for the Quadrangles containing these areas had not as yet been produced. It was also intended to obtain information about the martian atmosphere through radiometric measurements of the shadows associated with geological features, especially bowl-shaped craters. Although a number of shadows were identified in the narrow field of view imagery from Mariner VI, in particular Frame 6N22, the lack of available shadows is a direct result of the large diameter/depth ratios observed for Mars compared to Mercury and the Moon (Cintala, 1976). The diameter to depth ratio for craters near 10 km in diameter is approximately 8 times larger while for craters near 100 km in diameter it is approximately 3 times larger. The lack of Mariner IX bi-band image data further inhibited the evaluation of atmospheric phenomena.

SECTION 6

REFERENCES

Adams, J. B. and T. B. McCord, "Mars: Interpretation of Spectral Reflectivity of Light and Dark Regions," Journal of Geophysical Research, Vol. 74, pp. 4857 (1969).

Arvidson, R. E., "Wind-Blown Streaks, Splotches and Associated Craters on Mars: Statistical Analysis of Mariner IX Photographs," ICARUS, Vol. 21, pp. 12 (1974).

Binder, A. B. and J. C. Jones, "Spectrophotometric Studies of the Photometric Function, Composition and Distribution of the Surface Materials of Mars," Journal of Geophysical Research, Vol. 77, pp. 3005 (1972).

Cambell, N. and B. Lucchitta, "A Limitation of First Generation Lunar Orbiter Negatives as Applied to Photoclinometry," NASA CR-100075, National Aeronautics and Space Administration (1968).

Cintala, M. J., J. W. Head and T. A. Mutch, "Craters on the Moon, Mars and Mercury: A Comparison of Depth/Diameter Characteristics," Reports of Accomplishments of Planetology Programs, 1975-1976, NASA TMX-3364, pp. 186 (1976).

Cutts, J. A., "Martian Spectral Reflectivity Properties from Mariner VII Observations," PhD Thesis, California Institute of Technology (1971).

Cutts, J. A., G. E. Danielson and M. E. Davies, "Mercator Photomap of Mars," Journal of Geophysical Research, Vol. 76, pp. 369 (1971).

Danielson, G. E. and D. R. Montgomery, "Calibration of the Mariner Mars 1969 Television Cameras," Journal of Geophysical Research, Vol. 76, pp. 418 (1971).

Davies, M. E. and R. A. Berg, "A Preliminary Control Net of Mars," Journal of Geophysical Research, Vol. 76, pp. 373 (1971).

de Vaucouleurs, G., J. Roth and C. Mulholland, "Preliminary Albedo Map of the South Polar Region," Journal of Geophysical Research, Vol. 78, pp. 4436 (1973).

Dzurisin, D. and G. E. Danielson, "Revised Albedo Measurements of Mercury," Reports of Accomplishments of Planetology Programs, 1975-1976, NASA TMX-3364, pp. 99 (1976).

Greeley, R., J. D. Iversen, J. B. Pollack, N. Udovich and B. White, "Wind Tunnel Studies of Martian Aeolian Processes," Proceedings of Royal Society of London, Series A, Vol. 341, pp. 331 (1974).

Greeley, R., J. D. Iversen, J. B. Pollack, N. Udovich and B. White, "Wind Tunnel Simulations of Light and Dark Streaks on Mars," Science, Vol. 184, pp. 847 (1974).

Hunt, G. R. and J. W. Salisbury, "Visible and Near-Infrared Spectral of Minearls and Rocks: I. Silicate Minerals," Modern Geology, Vol. 1, pp. 283 (1970).

Hunt, G. R., J. W. Salisbury and C. J. Lenhoff, "Visible and Near-Infrared Spectral of Minerals and Rocks: III. Oxides and Hydroxides," Modern Geology, Vol. 2, pp. 195 (1971).

Kinzly, R. E. and J. J. Mazurowski, "Project SLOPE - A Study of Lunar Orbiter Photographic Evaluation: Techniques, Implementation and Accuracy," NASA CR-66493, NASA Langley Research Center (1967).

Kinzly, R. E., M. J. Mazurowski and T. M. Holladay, "Image Evaluation and Its Application to Lunar Orbiter," Applied Optics, Vol. 7, pp. 1577 (1968).

Lambiotte, J. J. and G. R. Taylor, "A Photometric Technique for Deriving Slopes from Lunar Orbiter Photography," Space Systems for Planetary Geology and Geophysics, American Astronautical Society, Science and Technology Series, Vol. 17, PR 205 (1967).

Masursky, H., et al., "Mariner IX Television Reconnaissance of Mars and Its Satellites: Preliminary Results," Science, 21 January 1972.

Meador, W. E. and W. R. Weaver, "A Photometric Function for Diffuse Reflection by Particulate Materials," NASA TND-7903, National Aeronautics and Space Administration (1975).

McCord, T. B., "Comparison of the Reflectivity and Color of Bright and Dark Regions on the Surface of Mars," Astrophysical Journal, Vol. 156, pp. 79 (1969).

McCord, T. B., and J. B. Adams, "Spectral Reflectivity of Mars," Science, Vol. 163, p. 1058 (1969).

McCord, T. B. and Westphal, "Mars: Narrow Band Photometry from 0.3 to 2.5 microns of the Surface Regions During the 1969 Apparition," Astrophysical Journal, Vol. 168, pp. 141 (1971).

Minnaert, M., "The Reciprocity Principle in Lunar Photometry," Astrophysical Journal, Vol. 93, pp. 403 (1941).

Nicodemus, F. E., "Chapter 8, Radiometry," Applied Optics and Optical Engineering, Vol. IV, R. Kingslake, Ed. (1967).

Piech, K. R., and J. E. Walker, "Interpretation of Soils," Photogrammetric Engineering, Vol. 40, pp. 87 (1974).

Pohn, H. A. and Wildey, R. L., "A Photoelectric-Photographic Study of the Normal Albedo of the Moon," Contributions to Astrogeology, Geological Survey Professional Paper 599-E (1970).

Pollack, J. B. and C. Sagan, "An Analysis of Martian Photometry and Polarimetry," Smithsonian Astrophysical Observatory, Special Report No. 258, (1967).

Rindfleisch, T., "Photometric Method for Lunar Topography," Photogrammetric Engineering, Vol. 32, pp. 262 (1966).

Salisbury, J. W. and G. R. Hunt, "Martian Surface Materials: Effect of Particle Size on Spectral Behavior," Science, Vol. 161, pp. 365 (1968).

Schultz, P. H., "Comparison of Lunar and Planetory Imagery," Reports of Accomplishments of Planetology Programs, 1975-1976, NASA TMX-3364, pp. 73 (1976).

Thorpe, T. E., "Mariner IX Photometric Observation of Mars from November 1971 through March 1972," ICARUS, Vol. 20, pp. 482 (1973).

Ververka, J., Sagan, C., L. Quam, R. Tucker and B. Eross, "Variable Features on Mars III: Comparison of Mariner 1969 and Mariner 1971 Photography," ICARUS, Vol. 21, pp. 317 (1974).

Weaver, W. R., W. E. Meador and G. P. Wood, "Value of the Photometric Parameters of Mars and their Interpretation," NASA TMX-71949, NASA Langley Research Center (1974).

Young, A. T. and S. A. Collins, "Photometric Properties of the Mariner Cameras and of Selected Regions of Mars," Journal of Geophysical Research, Vol. 76, pp. 432 (1971).

Young, A. T., "Television Photometry: The Mariner IX Experience," ICARUS, Vol. 21, pp. 262 (1974).

APPENDIX

ANALYSIS SOFTWARE

This appendix describes three items of analysis software which were prepared during the course of this study. The principal software package consisted of the main program written in Fortran language and an associated subroutine, EPIC, written in Assembly language. Listings of the main program and subroutines programs are included in Figures A-1 and A-2 respectively. The purpose of this program is to retrieve a rectangular array of reflectance data from digital tapes of Mariner imagery provided by JPL and compute the mean, standard deviation, minimum and maximum of the reflectivities in the array. The data required is retrieved from the digital tapes using the Subroutine FPIC and subsequently analyzed by the main program whose listing is included in Figure A-1. In addition to computing the basic statistics, this main program also has the option of computing a histogram of the reflectivity values in the specified array.

Subroutine FPIC retrieves each element in a rectangular array located within the digital TV picture data for subsequent processing by the main program. The rectangular area of interest is defined by the following calling sequence:

CALL FPIC (NLS, NSS, NSE, NOL, ARRAY, NLA, NSA, RFAC) where:

NLS: is the line number within the picture where data retrieval begins

NSS: is the sample number within the line where data retrieval begins

```
C     THIS PROGRAM CALCULATES THE STATISTICS OF A RECTANGULAR IMAGE ARRAY
C     SUPPLIED BY SUBROUTINE FPIC.
C
ISN 0002      DIMENSION R(25,25),IHIST(15)
ISN 0003      REAL*8 TARGID
ISN 0004      DATA IOPT/0/
ISN 0005    1 FORMAT(A8,50X,4I4,F4.0,I2)
ISN 0006    9 FORMAT(1H1)
ISN 0007   10 FORMAT(6X 'TARGET IDENTIFICATION= ',A8,'    INITIAL LINE NO.=',I4,
             *'  INITIAL SAMPLE NO.=',I4,'  FINAL SAMPLE NO.=',I4,'  NO. OF LINE
             *S=',I4 /// 13X 'PERCENT REFLECTANCE: MINIMUM=',F6.3,'  MAXIMUM=',
             *F6.3,'  AVERAGE=',F6.3,'  STANDARD DEVIATION=',F8.5 ///
             *13X 'HISTOGRAM: CLASS INTERVAL=',F6.3,// 16X 'CLASS NO.      ',
             *15(I3,1X) / 16X 'NO. OF PIXELS  ',15(I3,1X) /  16X 'TOTAL NO. OF P
             *IXELS=',I5 /////)
ISN 0008   11 FORMAT(6X 'TARGET IDENTIFICATION= ',A8,'    INITIAL LINE NO.=',I4,
             *'  INITIAL SAMPLE NO.=',I4,'  FINAL SAMPLE NO.=',I4,'  NO. OF LINE
             *S=',I4 /// 13X 'PERCENT REFLECTANCE: MINIMUM=',F6.3,'  MAXIMUM=',
             *F6.3,'  AVERAGE=',F6.3,'  STANDARD DEVIATION=',F8.5 // 13X 'TOTAL
             *NO. OF PIXELS=',I5 /////)
ISN 0009      ICASE=-1
ISN 0010      NLA=25
ISN 0011      NSA=25
ISN 0012   50 READ(5,1,END=100) TARGID,NLS,NSS,NSE,NOL,RFAC,IOPT
ISN 0013      ICASE=ICASE+1
C
C     OBTAIN REFLECTANCE DATA ARRAY 'R'
C
ISN 0014      CALL FPIC(NLS,NSS,NSE,NOL,R,NLA,NSA,RFAC)
C
C     COMPUTE THE AVERAGE, STANDARD DEVIATION, MINIMUM AND MAXIMUM OF
C     THE 'R' ARRAY
C
ISN 0015      SUM=0.0
ISN 0016      SSQ=0.0
ISN 0017      RMIN=100.
ISN 0018      RMAX=0.0
ISN 0019      NOS=NSE-NSS+1
ISN 0020      NTOT=NOS*NOL
ISN 0021      DO 60 I=1,NOL
ISN 0022      DO 60 J=1,NOS
ISN 0023      RT=R(J,I)
ISN 0024      IF(RT.GE.RMIN) GO TO 55
ISN 0026      RMIN=RT
ISN 0027   55 IF(RT.LE.RMAX) GO TO 59
ISN 0029      RMAX=RT
ISN 0030   59 SUM=SUM+RT
ISN 0031   60 SSQ=SSQ+RT**2
ISN 0032      RAVE=SUM/FLOAT(NTOT)
ISN 0033      RSTD=SQRT((SSQ-FLOAT(NTOT)*RAVE**2)/FLOAT(NTOT-1))
ISN 0034      IF(IOPT.EQ.0)GO TO 80
C
C     COMPUTE HISTOGRAM
C
ISN 0036      NI=RFAC*(RMAX-RMIN)/15.
ISN 0037      CINT=FLOAT(NI+1)/RFAC
ISN 0038      DO 65 I=1,15
ISN 0039   65 IHIST(I)=0
ISN 0040      DO 70 I=1,NOL
ISN 0041      DO 70 J=1,NOS
ISN 0042      N=(R(J,I)-RMIN)/CINT +1.0
ISN 0043   70 IHIST(N)=IHIST(N)+1
ISN 0044      IF(MOD(ICASE,4).EQ.0)WRITE(6,9)
ISN 0046      WRITE(6,10) TARGID,NLS,NSS,NSE,NOL,RMIN,RMAX,RAVE,RSTD,CINT,
             *(I,I=1,15),(IHIST(I),I=1,15),NTOT
ISN 0047      GO TO 50
ISN 0048   80 IF(MOD(ICASE,4).EQ.0)WRITE(6,9)
ISN 0050      WRITE(6,11) TARGID,NLS,NSS,NSE,NOL,RMIN,RMAX,RAVE,RSTD,NTOT
ISN 0051      GO TO 50
ISN 0052  100 STOP
ISN 0053      END
```

Figure A-1 IMAGE STATISTICS MAIN PROGRAM LISTING

```
SYMBOL   INTERNAL STATEMENT NUMBERS
I        0021  0023  0038  0039  0040  0042  0046  0046  0046  0046  0046  0046
J        0022  0023  0041  0042
N        0042  0043  0043
R        0002  0014  0023  0042
NI       0036  0037
RT       0023  0024  0026  0027  0029  0030  0031
MOD      0044  0048
NLA      0010  0014
NLS      0012  0014  0046  0050
NOL      0012  0014  0020  0021  0040  0046  0050
NOS      0019  0020  0022  0041
NSA      0011  0014
NSE      0012  0014  0019  0046  0050
NSS      0012  0014  0019  0046  0050
SSQ      0016  0031  0031  0033
SUM      0015  0030  0030  0032
CINT     0037  0042  0046
FPIC     0014
IOPT     0004  0012  0034
NTOT     0020  0032  0033  0033  0046  0050
RAVE     0032  0033  0046  0050
RFAC     0012  0014  0036  0037
RMAX     0018  0027  0029  0036  0046  0050
RMIN     0017  0024  0026  0036  0042  0046  0050
RSTD     0033  0046  0050
SQRT     0033
FLOAT    0032  0033  0033  0037
ICASE    0009  0013  0013  0044  0048
IHIST    0002  0039  0043  0043  0046
TARGID   0003  0012  0046  0050


LABEL    DEFINED    REFERENCES
   1     0005       0012
   9     0006       0044  0048
  10     0007       0046
  11     0008       0050
  50     0012       0047  0051
  55     0027       0024
  59     0030       0027
  60     0031       0021  0022
  65     0039       0038
  70     0043       0040  0041
  80     0048       0034
 100     0052       0012


   LABEL   ADDR          LABEL   ADDR          LABEL   ADDR          LABEL   ADDR

      50   000DF6           55   000ED8           59   000EE4           60   000EEE
      65   000FFA           70   001054           80   001144          100   0011D4

*STATISTICS*      SOURCE STATEMENTS =       52 ,PROGRAM SIZE =      4608
```

Figure A-1 (Cont'd)

```
                                        1 * THIS SUBROUTINE WAS CREATED TO PROCESS THE MARS MARINER TV DATA . IT  00000100
                                        2 *       BASICALLY COPIES A TAPE FILE TO A DISK ON THE FIRST CALL NAD    00000200
                                        3 *       THEN ACCESSES THE DISK IN DIRECT MODE TO FIND SQUARES OF THE    00000300
                                        4 *       PICTURE AS REQUESTED BY THE CALLING PROGRAM                     00000400
                                        5         PRINT NOGEN                                                     00000500
000000                                  6 FPIC    CSECT                                                           00000600
                              00000     7         USING *,15                                                      00000700
                                        8         SAVE  (14,12),,FPIC_DON_SPARROW                                 00000800
00001A 18ED                            14         LR    14,13          CHAIN THE SAVE AREAS                     00000900
00001C 41D0 F030              00030    15         LA    13,SAVE                                                 00001000
000020 50DE 0008              00008    16         ST    13,8(14)                                                00001100
000024 50ED 0004              00004    17         ST    14,4(13)                                                00001200
000028 47F0 F58C              0058C    18         B     FPIC1                                                   00001300

                                       20         DROP  15                                                      00001500
                              00030    21         USING SAVE,13                                                 00001600
000030                                 22 SAVE     DS    9D                                                      00001700
                                       23 TDCB     DCB   DDNAME=TAPE,DSORG=PS,MACRF=(R),EODAD=EOT,SYNAD=TERR,    *00001800
                                                         BUFNO=0                                                 00001900
                                       74 DDCB     DCB   DDNAME=DISK,DSORG=PS,MACRF=(WL),EODAD=EOD,SYNAD=DERR,   *00002000
                                                         RECFM=F,BUFNO=0,DEVD=DA                                 00002100
                                      125 DDCBI    DCB   DDNAME=DISK,DSORG=DA,MACRF=(RKC),EODAD=EODI,SYNAD=DERRI,*00002200
                                                         RECFM=F,OPTCD=E,LIMCT=1000,BUFNO=0                      00002300
000180                                174 KEY      DS    F                                                       00002400
000184                                175 BUFFER   DS    CL1000                                                  00002500
                              00001   176 TRUE     EQU   1                                                       00002600
                              00000   177 FALSE    EQU   0                                                       00002700
00056C 00                             178 ENDOFHDRS DC    AL1(FALSE)                                              00002800
000570                                179 TEMP     DS    D                                                       00002900
000578                                180 NUMBEROFLINESPERPICTURE DS F                                           00003000
00057C                                181 NUMBEROFSAMPLESPERLINE DS F                                            00003100
000580                                182 NOOFLABELRECORDS DS F                                                  00003200
000584                                183 NUMBEROFRECORDSONTAPE DS F                                             00003300
000588 42000000                       184 FLOATPAT DC     X'42000000'                                            00003400

00058C                                186 FPIC1    DS    0H                                                      00003600
00058C 1881                           187         LR    8,1            SAVE THE PARM ADDRESS                    00003700
00058E 9501 D53C      0056C           188         CLI   ENDOFHDRS,TRUE       FIRST ENTRY ?                    00003800
000592 4780 D6FE              0072E   189         BE    FPIC2          NO - BRANCH                              00003900

                                      191         OPEN  (TDCB,(INPUT))       YES - OPEN THE INPUT TAPE        00004100
                              00000   197         USING IHADCB,1                                                00004200
0005A2 4110 D048              00078   198         LA    1,TDCB                                                  00004300
0005A6 9110 1030      00030           199         TM    DCBOFLGS,X'10'       WAS OPEN ALRIGHT ?                00004400
0005AA 47E0 D836              00866   200         BNO   TOERR           NO - BRANCH                            00004500

0005AE 4140 D0A0              000D0   202         LA    4,DDCB           YES - GET  THE @ OF THE DISK DCB      00004700
                                      203         DROP  1                                                       00004800

0005B2 1B22                           205         SR    2,2              CLEAR THE RECORD COUNTER REGISTER      00005000
0005B4 47F0 D596              005C6   206         B     READTAPE         START THE COPY                         00005100

0005B8                                208 COPYTODISK DS 0H                                                      00005300
                                      209         CHECK CODECB           SEE IF DISK WRITE WAS ALRIGHT          00005400

0005C6                                215 READTAPE DS     0H                                                    00005600
0005C6 D703 D5A0 D5A0 005D0 005D0     216         XC    TDECB,TDECB      CLEAR THE DECB FOR A READ             00005700
                                      217         READ  TDECB,SF,TDCB,BUFFER+4,'S' READ A TAPE RECORD          00005800
0005EE 4122 0001              00001   230         LA    2,1(2)           COUNT THE RECORD                       00005900

0005F2 9501 D53C      0056C           232         CLI   ENDOFHDRS,TRUE       ARE WE IN THE DATA RECORDS ?      00006100
0005F6 4780 D624              00654   233         BE    DATARECORD       YES - BRANCH                           00006200

                                      235         CHECK TDECB            NO - SEE IF THE TAPE READ WAS ALRIGHT  00006400
000608 4110 D158              00188   240         LA    1,BUFFER+4       SET BASE FOR USING                     00006500
00060C 5920 D938              00968   241         C     2,=F'1'          IS THIS THE FIRST LABEL RECORD ?       00006600
000610 4720 D600              00630   242         BH    NOT1STLABEL      NO - BRANCH                            00006700

                              00000   244         USING LABEL,1          YES - GET NS AND NL FOR THIS TAPE      00006900
000614 F273 D540 1020 00570   00020   245         PACK  TEMP,NL          CONVERT FROM EBCDIC TO BINARY          00007000
00061A 4F00 D540              00570   246         CVB   0,TEMP                                                  00007100
00061E 5000 D548              00578   247         ST    0,NUMBEROFLINESPERPICTURE                               00007200

000622 F273 D540 1024 00570   00024   249         PACK  TEMP,NS          REPEAT FOR NS                          00007400
000628 4F00 D540              00570   250         CVB   0,TEMP                                                  00007500
00062C 5000 D54C              0057C   251         ST    0,NUMBEROFSAMPLESPERLINE                                00007600
                                      252         DROP  1                                                       00007700

                                      254 * THE LAST LOGICAL LABEL RECORD HAS AN 'L' IN THE LAST BYTE -          00007900
                                      255 *       NO ADDITIONAL LABEL RECORDS WILL FOLLOW THIS ONE               00008000
000630                                256 NOT1STLABEL DS 0H                                                     00008100
000630 4100 0005              00005   257         LA    0,5                                                     00008200
```

Figure A-2 SUBROUTINE FPIC LISTING

```
000634                                  259 CHECKFORLASTLABEL DS 0H                                          00008400
                                 00000  260          USING LABELREC,1                                        00008500
000634 9503 1047       00047     261          CLI   ENDOFLABELCHECK,C'L'     IS THIS THE LAST LABEL RECORD ? 00008600
000638 4780 D618              00648  262          BE    SETLASTLABELRECORD                                    00008700

00063C 4111 0048              00048  264          LA    1,72(1)          NO - BUMP INDEX                      00008900
000640 4600 D604              00634  265          BCT   0,CHECKFORLASTLABEL LOOK ALLL LABEL RECORDS IN BLOCK  00009000
000644 47F0 D596              005C6  266          B     READTAPE         GET NEXT LABEL RECORD                00009100

000648                                  268 SETLASTLABELRECORD DS 0H                                         00009300
000648 9201 D53C       0056C     269          MVI   ENDOFHDRS,TRUE       YES - SET SWITCH                     00009400
00064C 5020 D550              00580  270          ST    2,NOOFLABELRECORDS  SAVE THE NUMBER OF LABEL RECORDS   00009500
000650 47F0 D596              005C6  271          B     READTAPE       CONTINUE                              00009600
                                     272          DROP  1                                                    00009700

000654                                  274 DATARECORD DS  0H                                                00009900
                                        275          CHECK TDECB          SEE IF TAPE READ WAS ALRIGHT       00010000

                                 00000  281          USING IHADCB,4                                          00010200
000662 9110 4030       00030     282          TM    DCBOFLGS,X'10'       IS THE DISK DCB OPEN ?             00010300
000666 4710 D656              00686  283          BO    DDCBO            YES - BRACNH                       00010400

00066A 5800 D54C              0057C  285          L     0,NUMBEROFSAMPLESPERLINE NO - SET THE BLKSIZE       00010600
00066E 4000 403E              0003E  286          STH   0,DCBBLKSI                                          00010700

                                     288          OPEN  (DDCB,(OUTPUT))      OPEN THE DCB                    00010900
00067E 9110 4030       00030     294          TM    DCBOFLGS,X'10'       WAS THE OPEN ALRIGHT ?             00011000
000682 47E0 D846              00876  295          BNO   DOERR            NO - BRANCH                        00011100

000686                                  297 DDCBO     DS    0H                                               00011300
                                        298 * THE KEY OF EACH RECORD IS THE RECORD NUMBER OR LINE NUMBER WHICH  00011400
                                        299 *         RANGES FROM 1 TO NUMBEROFLINESPERPICTURE                 00011500
000686 1802                             300          LR    0,2              COMPUTE THE KEY                   00011600
000688 5800 D550              00580  301          S     0,NOOFLABELRECORDS                                   00011700
00068C 5000 D154              00184  302          ST    0,BUFFER         SET THE KEY IN FRONT OF THE RECORD  00011800

000690 D703 D66C D66C 0069C 0069C     304          XC    CDDECB,CDDECB        CLEAR THE DECB FOR DISK WRITE  00012000
                                     305          WRITE CDDECB,SF,DDCB,BUFFER    WRITE THE RECORD TO DISK  00012100

0006BA 47FF D68E              006BE  319          B     *+4(15)          CHECK THE RETURN CODE FROM WRITE    00012300
0006BE 47F0 D588              00588  320          B     COPYTODISK                                           00012400
0006C2 47F0 D588              00588  321          B     COPYTODISK                                           00012500
0006C6 47F0 D588              00588  322          B     COPYTODISK                                           00012600

                                     324          ABEND 69,DUMP          WRITE WAS NO GOOD                   00012800
                                     332          DROP  4                                                    00012900

0006DA                                  334 EOT       DS    0H                                               00013100
0006DA 0620                             335          BCTR  2,0              (2) = NUMBER OF RECORDS ON TAPE  00013200
0006DC 5020 D554              00584  336          ST    2,NUMBEROFRECORDSONTAPE                              00013300

0006E0 5820 D550              00580  338          S     2,NOOFLABELRECORDS  DOES IT CHECK WITH NL IN HEADER ? 00013500
0006E4 5920 D548              00578  339          C     2,NUMBEROFLINESPERPICTURE                            00013600
0006E8 4780 D6CA              006FA  340          BE    TDOK             YES - BRANCH                        00013700

                                     342          ABEND 169,DUMP                                             00013900

0006FA                                  351 TDOK      DS    0H                                               00014100
                                        352          CLOSE (TDCB,,DDCB)  CLOSE THE DCBS                       00014200

00070A 4120 D0E8              00118  361          LA    2,DDCBI           SET DATA TO READ DISK              00014400
                              00000  362          USING IHADCB,2                                             00014500

00070E 5800 D54C              0057C  364          L     0,NUMBEROFSAMPLESPERLINE                             00014700
000712 4000 2052              00052  365          STH   0,DCBLRECL                                           00014800
000716 4000 203E              0003E  366          STH   0,DCBBLKSI                                           00014900

                                     368          OPEN  (DDCBI,(INPUT))      READY DISK FOR INPUT MODE       00015100

000726 9110 2030       00030     375          TM    DCBOFLGS,X'10'       WAS RE-OPEN ALRIGHT ?              00015300
00072A 47E0 D856              00886  376          BNO   DOOERR           NO - BRANCH                        00015400
                                     377          DROP  2                                                    00015500

                                        379 * WE END UP AT THIS POINT AFTER THE TAPE IS COPIED TO THE DISK ON THE 00015700
                                        380 *         FIRST CALL, OR IMMEDIATELY ON THE SECOND AND SUBSEQUENT CALLS 00015800
00072E                                  381 FPIC2     DS    0H                                               00015900
                              00000  382          USING PARMLIST,8                                           00016000
00072E 9825 8000              00000  383          LM    2,5,NLS          GET THE ADDRESSES OF THE PARMS      00016100
000732 5822 0000              00000  384          L     2,0(2)                                               00016200
000736 5833 0000              00000  385          L     3,0(3)                                               00016300
00073A 5844 0000              00000  386          L     4,0(4)                                               00016400
00073E 5855 0000              00000  387          L     5,0(5)                                               00016500

000742 1222                             389          LTR   2,2              IS START LINE NUMBER POSITIVE ?   00016700
000744 47D0 D986              00886  390          BNP   A269             NO - BRANCH                         00016800

000748 1812                             392          LR    1,2                                                00017000
00074A 1A15                             393          AR    1,5                                                00017100
00074C 5910 D548              00578  394          C     1,NUMBEROFLINESPERPICTURE IS END LINE # IN PICTURE ? 00017200
000750 4720 D896              008C6  395          BH    A369             NO - BRANCH                         00017300

000754 1233                             397          LTR   3,3              IS THE START SAMPLE POSITIVE ?    00017500
000756 47D0 D8A6              008D6  398          BNP   A469             NO - BRANCH                         00017600

00075A 1934                             400          CR    3,4              IS START SAMPLE LESS THAN END SAMPLE ? 00017800
00075C 4780 D8B6              008E6  401          BNL   A569             NO - BRANCH                         00017900

000760 5940 D54C              0057C  403          C     4,NUMBEROFSAMPLESPERLINE IS END SAMPLE ON A LINE ?   00018100
000764 4720 D8C6              008F6  404          BH    A669             NO - BRANCH                         00018200
```

Figure A-2 (Cont'd)

```
000768 1244                          406          LTR   4,4          IS END SAMPLE WITHIN A LINE ?                    00018400
00076A 47D0 D8D6          00906      407          BNP   A769         NO - BRANCH                                      00018500

00076E 1255                          409          LTR   5,5          IS THE NUMBER OF LINES IN SQUARE POSITIVE        00018700
000770 47D0 D8E6          00916      410          BNP   A869         NO - BRANCH                                      00018800

000774 5860 8014          00014      412          L     6,NLA        GET THE DIMENSIONS OF RECEIVING ARRAY            00019000
000778 5866 0000          00000      413          L     6,0(6)        # OF COLUMNS IN RECEIVING ARRAY                 00019100
00077C 5870 8018          00018      414          L     7,NSA                                                        00019200
000780 5877 0000          00000      415          L     7,0(7)        # OF ROWS, E.G. ARRAY 'A' IS 'A(NSA,NLA)'   00019300

000784 1814                          417          LR    1,4                                                          00019500
000786 1813                          418          SR    1,3                                                          00019600
000788 4111 0001          00001      419          LA    1,1(1)        (1) IS THE NUMBER OF SAMPLES TO PUT IN A       00019700
                                     420 *                                PUT IN A ROW OF 'A' ARRAY                00019800
00078C 1917                          421          CR    1,7          IS THE REQUEST FITTABLE IN ARRAY ROWS ?          00019900
00078E 4720 D8F6          00926      422          BH    A969         NO - BRANCH                                      00020000

000792 1956                          424          CR    5,6           IS REQUEST FITTABLE IN ARRAY COLUMNS ?         00020200
000794 4720 D906          00936      425          BH    A1069        NO - BRANCH                                      00020300

000798 5810 801C          0001C      427          L     1,RFAC       GET THE SCALE FACTOR                             00020500
00079C 7821 0000          00000      428          LE    2,0(1)                                                        00020600

0007A0 58C0 8010          00010      430          L     12,A                                                         00020800
0007A4 18A7                          431          LR    10,7                                                         00020900
0007A6 89A0 0002          00002      432          SLL   10,2         NSA*4 - SIZE OF ROW IN ARRAY                   00021000

0007AA 181A                          434          LR    1,10                                                         00021200
0007AC 0650                          435          BCTR  5,0                                                          00021300
0007AE 1C05                          436          MR    0,5                                                          00021400
0007B0 4181 C000          00000      437          LA    11,0(1,12)   A + ((NSA-1)*4)*(NOL-1) - @ OF LAST ROW IN  00021500
                                     438 *                                ARRAY TO SET FROM DATA                   00021600

0007B4 0630                          440          BCTR  3,0          READY (3) FOR LOOP AT SAMPLELOOP                 00021800

0007B6 4160 0001          00001      442          LA    6,1          INCREMENT FOR SAMPLE LOOP                        00022000
0007BA 0640                          443          BCTR  4,0                                                          00022100
0007BC 4174 D154          00184      444          LA    7,BUFFER(4)  @ OF LAST SAMPLE IN RECORD TO PROCESS            00022200

0007C0                               446 LINELOOP DS    0H                                                          00022400
0007C0 5020 D150          00180      447          ST    2,KEY         SET OF RECORD WE WANT TO READ                  00022500

0007C4 D703 D7A0 D7A0 007D0 007D0    449          XC    FDECB,FDECB  READY FOR FETCH READ                          00022700
                                     450          READ  FDECB,DK,DDCBI,BUFFER,'S',KEY,TEMP FETCH DATA FROM DISK  00022800
                                     464          CHECK FDECB        SEE IF THE READ WAS ALRIGHT ?                   00022900

000800 1B11                          470          SR    1,1          (1) IS INDEX TO ROW IN A ARRAY                  00023100
000802 4143 D154          00184      471          LA    4,BUFFER(3)  (4) IS PTR TO DAZTA ITEM TO PROCESS             00023200

000806                               473 SAMPLELOOP DS  0H                                                          00023400
000806 4304 0000          00000      474          IC    0,0(4)       GET THE DATA                                    00023500
00080A 4200 D559          00589      475          STC   0,FLOATPAT+1 FLOAT IT                                        00023600
00080E 7800 D558          00588      476          LE    0,FLOATPAT                                                   00023700
000812 3D02                          477          DER   0,2          SCALE IT                                        00023800
000814 7001 C000          00000      478          STE   0,0(1,12)    STORE IT IN 'A' ARRAY                           00023900
000818 4111 0004          00004      479          LA    1,4(1)       BUMP ROW PTR                                    00024000
00081C 8746 D7D6          00806      480          BXLE  4,6,SAMPLELOOP      FINISH THE ROW                          00024100

000820 4122 0001          00001      482          LA    2,1(2)       BUMP DESIRED RECORD KEY                         00024300
000824 87CA D790          007C0      483          BXLE  12,10,LINELOOP      PROCESS ALL LINES IN SQUARE              00024400


000828 58DD 0004          00004      485          L     13,4(13)                                                     00024600
                                     486          RETURN (14,12),RC=0 RETURN                                       00024700




000836                               491 EOD      DS    0H                                                          00024900
                                     492          ABEND 1169,DUMP                                                  00025000

000846                               501 DERR     DS    0H                                                          00025200
                                     502          ABEND 1269,DUMP                                                  00025300

000856                               511 TERR     DS    0H                                                          00025500
                                     512          ABEND 1369,DUMP                                                  00025600

000866                               521 TOERR    DS    0H                                                          00025800
                                     522          ABEND 1469,DUMP                                                  00025900

  LOC  OBJECT CODE    ADDR1 ADDR2  STMT   SOURCE STATEMENT                                  ASM H V 05 11.17 07/14/77

000876                               531 DOERR    DS    0H                                                          00026100
                                     532          ABEND 1569,DUMP                                                  00026200

000886                               541 DOOERR   DS    0H                                                          00026400
                                     542          ABEND 1669,DUMP                                                  00026500

000896                               551 DERRI1   DS    0H                                                          00026700
                                     552          ABEND 1769,DUMP                                                  00026800

0008A6                               561 DERRI2   DS    0H                                                          00027000
                                     562          ABEND 1869,DUMP                                                  00027100
```

Figure A-2 (Cont'd)

```
0008B6                          571 A269     DS    0H                                                    00027300
                                572          ABEND 269,DUMP                                              00027400

0008C6                          581 A369     DS    0H                                                    00027600
                                582          ABEND 369,DUMP                                              00027700

0008D6                          591 A469     DS    0H                                                    00027900
                                592          ABEND 469,DUMP                                              00028000

0008E6                          601 A569     DS    0H                                                    00028200
                                602          ABEND 569,DUMP                                              00028300

0008F6                          611 A669     DS    0H                                                    00028500
                                612          ABEND 669,DUMP                                              00028600

000906                          621 A769     DS    0H                                                    00028800
                                622          ABEND 769,DUMP                                              00028900

000916                          631 A869     DS    0H                                                    00029100
                                632          ABEND 869,DUMP                                              00029200

000926                          641 A969     DS    0H                                                    00029400
                                642          ABEND 969,DUMP                                              00029500

000936                          651 A1069    DS    0H                                                    00029700
                                652          ABEND 1069,DUMP                                             00029800

000946                          661 EODI     DS    0H                                                    00030000
                                662          ABEND 1969,DUMP                                             00030100

000956                          671 DERRI    DS    0H                                                    00030300
                                672          ABEND 2069,DUMP                                             00030400

000000                          681 LABEL    DSECT                                                       00030600
000000                          682          DS    32X                                                   00030700
000020                          683 NL       DS    CL4                                                   00030800
000024                          684 NS       DS    CL4                                                   00030900
000028                          685          DS    32X                                                   00031000

000000                          687 LABELREC DSECT                                                       00031200
000000                          688          DS    71X                                                   00031300
000047                          689 ENDOFLABELCHECK DS C                                                 00031400

000000                          691 PARMLIST DSECT                                                       00031600
000000                          692 NLS      DS    A                                                     00031700
000004                          693 NSS      DS    A                                                     00031800
000008                          694 NSE      DS    A                                                     00031900
00000C                          695 NOL      DS    A                                                     00032000
000010                          696 A        DS    A                                                     00032100
000014                          697 NLA      DS    A                                                     00032200
000018                          698 NSA      DS    A                                                     00032300
00001C                          699 RFAC     DS    A                                                     00032400

                                701          DCBD  DSORG=PS                                              00032600
                                702**,***    IHB069 DEVD NOT SPECIFIED-ALL ASSUMED                       02-IHBER
                               1452          END                                                         00032700
000968 00000001                1453                =F'1'
```

CROSS REFERENCE

```
SYMBOL    LEN     VALUE   DEFN   REFERENCES
A         00004   000010  0696   0430
A1069     00002   000936  0651   0425
A269      00002   0008B6  0571   0390
A369      00002   0008C6  0581   0395
A469      00002   0008D6  0591   0398
A569      00002   0008E6  0601   0401
A669      00002   0008F6  0611   0404
A769      00002   000906  0621   0407
A869      00002   000916  0631   0410
A969      00002   000926  0641   0422
BUFFER    01000   000184  0175   0225  0240  0302  0313  0444  0458  0471
CDDECB    00004   00069C  0308   0210  0304  0304
CHECKFORLASTLABEL
          00002   000634  0259   0265
COPYTODISK
          00002   000588  0208   0320  0321  0322
DATARECORD
          00002   000654  0274   0233
DCBBIT0   00001 00000080  0714   0835  0851  0890  0908  0953  0963  0979  1020  1030  1042  1065  1096  1099  1101  1103
                                 1126  1129  1149  1154  1173  1210  1263  1286  1318  1322  1335  1430  1433  1443
DCBBIT1   00001 00000040  0715   0836  0852  0909  0917  0953  0963  0981  1021  1031  1044  1066  1068  1078  1096  1099
                                 1102  1103  1131  1149  1152  1154  1176  1177  1178  1213  1214  1263  1288  1324  1326
                                 1338  1382  1430  1435  1444
DCBBIT2   00001 00000020  0716   0837  0853  0910  0919  0963  0982  1022  1032  1045  1047  1048  1066  1068  1073  1079
                                 1096  1098  1105  1133  1156  1158  1181  1182  1183  1217  1218  1265  1291  1327  1343
                                 1385  1389  1430  1445
DCBBIT3   00001 00000010  0717   0801  0838  0854  0924  0966  0983  1023  1045  1048  1050  1066  1081  1106  1136  1156
                                 1160  1185  1186  1187  1221  1222  1265  1293  1295  1297  1329  1344  1385  1390  1430
DCBBIT4   00001 00000008  0718   0802  0855  0925  0969  0984  1024  1033  1082  1107  1137  1162  1168  1169  1190  1191
                                 1225  1226  1228  1229  1267  1300  1345  1385  1391
```

Figure A-2 (Cont'd)

```
DCBBIT5  00001 00000004  0719   0804  0856  0927  0970  0984  1025  1034  1083  1110  1112  1139  1162  1165  1166  1169
                               1194  1196  1197  1198  1232  1233  1234  1235  1267  1302  1305  1331  1347  1380
DCBBIT6  00001 00000002  0720   0806  0839  0857  0929  0971  0988  1026  1084  1086  1089  1110  1113  1140  1201  1202
                               1203  1204  1238  1239  1240  1241  1308  1349
DCBBIT7  00001 00000001  0721   0808  0840  0933  0973  0989  1027  1084  1087  1089  1115  1144  1206  1207  1244  1245
                               1247  1248  1333  1350  1392
DCBBLKSI 00002    00003E 1352   0286  0366
DCBFDAD  00008    000005 0735   0738
DCBLRECL 00002    000052 1414   0365
DCBOFLGS 00001    000030 1125   0199  0282  0294  0375
DCBSSID  00008    000000 0942   0945
DCBWTOID 00004    000000 0862   0877  0886
DDCB     00004    000DD0 0078   0202  0292  0312  0358
DDCBI    00004    000118 0130   0361  0372  0457  0462
DDCBO    00002    000686 0297   0283
DERR     00002    000846 0501   0111
DERRI    00002    000956 0671   0161
DOERR    00002    000876 0531   0295
DODERR   00002    000986 0541   0376
ENDOFHDRS
         00001    00056C 0178   0188  0232  0269
ENDOFLABELCHECK
         00001    000047 0689   0261
EOD      00002    000836 0491   0096
EODI     00002    000946 0661   0146
EOT      00002    0006DA 0334   0045
FALSE    00001 00000000 0177   0178
FDECB    00004    0007D0 0453   0449  0449  0465
FLOATPAT 00004    000588 0184   0475  0476
FPIC1    00002    00058C 0186   0018
FPIC2    00002    00072E 0381   0189
IHADCB   00001 00000000 0712   0197  0281  0362  0760  0784  0812  0831  0861  0941  1002  1053  1122  1254  1271  1275
                               1281  1370  1376  1400  1421
KEY      00004    000180 0174   0447  0460
LABEL    00001 00000000 0681   0244
LABELREC 00001 00000000 0687   0260
LINELOOP 00002    0007C0 0446   0483
NL       00004    000020 0683   0245
NLA      00004    000014 0697   0412
NLS      00004    000000 0692   0383
NOOFLABELRECORDS
         00004    000580 0182   0270  0301  0338
NOT1STLABEL
         00002    000630 0256   0242
NS       00004    000024 0684   0249
NSA      00004    000018 0698   0414
NUMBEROFLINESPERPICTURE
         00004    000578 0180   0247  0339  0394
NUMBEROFRECORDSONTAPE
         00004    000584 0183   0336
NUMBEROFSAMPLESPERLINE
         00004    00057C 0181   0251  0285  0364  0403
PARMLIST 00001 00000000 0691   0382
READTAPE 00002    0005C6 0215   0206  0266  0271
RFAC     00004    00001C 0699   0427
SAMPLELOOP
         00002    000806 0473   0480
SAVE     00008    000030 0022   0015  0021
SETLASTLABELRECORD
         00002    000648 0268   0262
TDCB     00004    000078 0027   0195  0198  0224  0356
TDECB    00004    0005D0 0220   0216  0216  0236  0276
TDOK     00002    0006FA 0351   0340
TEMP     00008    000570 0179   0245  0246  0249  0250  0461
TERR     00002    000856 0511   0060
TOERR    00002    000866 0521   0200
TRUE     00001 00000001 0176   0188  0232  0269
=F'1'    00004    000968 1453   0241


                        DIAGNOSTIC CROSS REFERENCE AND ASSEMBLER SUMMARY


  NO STATEMENTS FLAGGED IN THIS ASSEMBLY

OVERRIDING PARAMETERS-  LOAD
OPTIONS FOR THIS ASSEMBLY
  NODECK, OBJECT, LIST, XREF(SHORT), NORENT, NOTEST, BATCH, ALIGN, ESD, NORLD, LINECOUNT(55), FLAG(0), SYSPARM()
NO OVERRIDING DD NAMES

  327 CARDS FROM SYSIN     5496 CARDS FROM SYSLIB
  392 LINES OUTPUT           30 CARDS OUTPUT
```

Figure A-2 (Cont'd)

NSE: is the last sample within the line to be included in the retrieved data

NOL: is the number of consecutive lines for retrieval of data (including NLS)

These parameters define the rectangular area within the image.

ARRAY: is the array into which the retrieval data is put

NLA: is the second dimension of the array (the number of rows (lines) the array contains)

NSA: is the first dimension of the array (the number of columns (samples) the array contains)

These parameters define the array to receive the data.

RFAC: is a scale factor by which each sample is divided

Note: NLS, NSS, NSE, NOL, NLA, NSA are assumed to be INTEGER *4 arguments while ARRAY and RFAC are assumed to REAL *4 arguments and further, a previous statement:

DIMENSION ARRAY (NSA, NLA) is assumed to have been included in the program that uses FPIC, which is FORTRAN compatible.

The data to be manipulated by FPIC is assumed to reside on a tape defined by a DD card as follows:

```
//GO.TAPE DD DSN=name,DISP=OLD,UNIT=2400,
// VOL=SER=volser,DCB=(RECFM=U,BLKSIZE=1000)
// LABEL=(file #,SL,,IN)
```

As part of FPIC's operation, another DD card is required as follows:

```
//GO.DISK DD DSN=&&TEMP,DISP=NEW,UNIT=SYSDA,
// DCB =(DSØRG=DA,KEYLEN=4,SPACE =(TRK,(300,10))
```

The operation of FPIC is as follows:

1) The first call to the subroutine causes the data (not the label) records to be copied from the tape to the disk data set as a direct access file with the line number as the record key.

2) The required lines (records) are then read from the disk, the sample bytes are extracted, floated, scaled and stored in ARRAY.

Certain operational errors will cause user abends. These are listed below.

Abend	Reason
69	disk write rejected
169	no. of data records ≠ NL in header
269	start line number negative
369	requested number of lines > NL in header
469	start sample # negative
569	start sample # > end sample #
669	end sample # > NS in header
769	end sample # negative
869	number of lines in square (NOL) negative
969	(end sample # - start sample #)>NS in A array
1069	number of lines (NOL)> NL in A array
1169	EODAD on disk (write)
1269	disk I/O error (write)
1369	Tape I/O error
1469	unable to open tape data set dcb

1569	unable to open disk data set (write) dcb (write)
1669	unable to open disk data set dcb (read)
1969	end of dataon disk data set (read)
2069	I/O error on disk data set (read)

A program was written to compute the average spectral reflectance within a particular spectral band given the spectral reflectivity of the sample and the spectral transmission of the filter under consideration. Figure A-3 is a listing of this program which was written in Fortran language. Each of the steps in the program is clearly identified by comments and no further explanation is required. As utilized in the present study, FIL (1,J) through FIL (6,J) represent the six spectral transmissions for the blue, green, red filters of Mariner VI and Marinter VII respectively. RBAR represent the average spectral reflectivity of the sample in each of these spectral bands and the value of RATIO (1) and RATIO (2) are the red-to-blue and red-to-green reflectivity ratios for the Mariner VI spectral bands while RATIO (3) and RATIO (4) are the corresponding values for the Mariner VII spectral bands.

```
C
C ***************************************************************************
C **                                                                       **
C **  THIS PROGRAM COMPUTES THE AVERAGE SPECTRAL REFLECTANCE OF A SAMPLE   **
C **  FOR SPECTRAL BANDS GIVEN THE SPECTRAL TRANSMISSION AND THE           **
C **  SAMPLE REFLECTANCE.                                                  **
C **                                                                       **
C ***************************************************************************
C
ISN 0002        DIMENSION FIL(6,151),R(151),SID(20),RBAR(6),RATIO(4)
ISN 0003       1 FORMAT(4(10X,F10.0))
ISN 0004       2 FORMAT(20A4)
ISN 0005       3 FORMAT(1H1,9X,20A4//15X 'AVERAGE REFLECTANCE'/ 20X 'BAND',2X,'1',
              *8X,'2',8X,'3',8X,'4',8X,'5',8X,'6'// 20X, 6F9.3 //15X 'REFLECTANCE
               * RATIOS', 10X, 4F8.3, 4(/))
ISN 0006       4 FORMAT(   10X,20A4//15X 'AVERAGE REFLECTANCE'/ 20X 'BAND',2X,'1',
              *8X,'2',8X,'3',8X,'4',8X,'5',8X,'6'// 20X, 6F9.3 //15X 'REFLECTANCE
               * RATIOS', 10X, 4F8.3, 4(/))
ISN 0007        CALL CLEAR(FIL(1,1),FIL(6,151))
C
C  ***************************************************************************
C  *                                                                         *
C  *  READ SPECTRAL TRANSMISSION DATA                                        *
C  *                                                                         *
C  ***************************************************************************
C
ISN 0008        READ(5,1)  (FIL(1,J),J=2,151)
ISN 0009        READ(5,1)  (FIL(2,J),J=2,151)
ISN 0010        READ(5,1)  (FIL(3,J),J=2,151)
ISN 0011        READ(5,1)  (FIL(4,J),J=1,151)
ISN 0012        READ(5,1)  (FIL(5,J),J=1,151)
ISN 0013        READ(5,1)  (FIL(6,J),J=1,151)
C
C  ***************************************************************************
C  *                                                                         *
C  *  NORMALIZE SPECTRAL TRANSMISSION DATA                                   *
C  *                                                                         *
C  ***************************************************************************
C
ISN 0014        DO 30 I=1,6
ISN 0015        S=0.0
ISN 0016        DO 22 J=1,151
ISN 0017       22 S=S+FIL(I,J)
ISN 0018        DO 24 J=1,151
ISN 0019       24 FIL(I,J)=FIL(I,J)/S
ISN 0020       30 CONTINUE
C
C  ***************************************************************************
C  *                                                                         *
C  *  READ SAMPLE SPECTRAL REFLECTANCE DATA                                  *
C  *                                                                         *
C  ***************************************************************************
C
ISN 0021        ICASE=0
ISN 0022       40 READ(5,2,END=70) SID
ISN 0023         ICASE=ICASE+1
```

Figure A-3 AVERAGE REFLECTIVITY MAIN PROGRAM LISTING

```
ISN 0024            READ(5,1) R
                C
                C  ***************************************************************************
                C  *                                                                         *
                C  *  DETERMINE AVERAGE SAMPLE REFLECTANCE FOR EACH SPECTRAL BAND            *
                C  *                                                                         *
                C  ***************************************************************************
                C
ISN 0025            DO 50 I=1,6
ISN 0026            RBAR(I)=0.0
ISN 0027            DO 45 J=1,151
ISN 0028         45 RBAR(I)=RBAR(I)+R(J)*FIL(I,J)
ISN 0029         50 CONTINUE
                C
                C  ***************************************************************************
                C  *                                                                         *
                C  *  COMPUTE RATIOS OF AVERAGE REFLECTANCES                                 *
                C  *                                                                         *
                C  ***************************************************************************
                C
ISN 0030            DO 55 N=1,4
ISN 0031         55 RATIO(N)=0.0
ISN 0032            IF(RBAR(1).GT.0.0) RATIO(1)=RBAR(3)/RBAR(1)
ISN 0034            IF(RBAR(2).GT.0.0) RATIO(2)=RBAR(3)/RBAR(2)
ISN 0036            IF(RBAR(4).GT.0.0) RATIO(3)=RBAR(6)/RBAR(4)
ISN 0038            IF(RBAR(5).GT.0.0) RATIO(4)=RBAR(6)/RBAR(5)
                C
                C  ***************************************************************************
                C  *                                                                         *
                C  *  PRINT OUTPUT DATA AND RECYCLE TO PROCESS NEXT CASE, IF ANY.            *
                C  *                                                                         *
                C  ***************************************************************************
                C
ISN 0040            IF(MOD(ICASE,5).NE.1) GO TO 60
ISN 0042            WRITE(6,3) (SID(K),K=1,20),(RBAR(I),I=1,6),(RATIO(N),N=1,4)
ISN 0043            GO TO 40
ISN 0044         60 WRITE(6,4) (SID(K),K=1,20),(RBAR(I),I=1,6),(RATIO(N),N=1,4)
ISN 0045            GO TO 40
                C
                C  ***************************************************************************
                C  *                                                                         *
                C  *  TERMINATE EXECUTION                                                    *
                C  *                                                                         *
                C  ***************************************************************************
                C
ISN 0046         70 STOP
ISN 0047            END
```

Figure A-3 (Cont'd)

```
   LABEL    ADDR                LABEL    ADDR                LABEL    ADDR        LABEL    ADDR

      22  001472                  24  00149C                  30  0014AA          40  0014C6
      45  00153A                  50  001550                  55  00155E          60  001626
      70  00167A

        *****F O R T R A N    C R O S S    R E F E R E N C E    L I S T I N G*****

SYMBOL  INTERNAL STATEMENT NUMBERS
I       0014  0017  0019  0019  0025  0026  0028  0028  0028  0042  0042  0042  0044  0044
        0044
J       0008  0008  0008  0009  0009  0009  0010  0010  0010  0011  0011  0011  0012  0012
        0012  0013  0013  0013  0016  0017  0018  0019  0019  0027  0028  0028
K       0042  0042  0042  0044  0044  0044
N       0030  0031  0042  0042  0042  0044  0044  0044
R       0002  0024  0028
S       0015  0017  0017  0019
FIL     0002  0007  0007  0008  0009  0010  0011  0012  0013  0017  0019  0019  0028
MOD     0040
SID     0002  0022  0042  0044
RBAR    0002  0026  0028  0028  0032  0032  0032  0034  0034  0034  0036  0036  0036
        0038  0038  0038  0042  0044
CLEAR   0007
ICASE   0021  0023  0023  0040
RATIO   0002  0031  0032  0034  0036  0038  0042  0044


LABEL   DEFINED   REFERENCES
    1   0003      0008  0009  0010  0011  0012  0013  0024
    2   0004      0022
    3   0005      0042
    4   0006      0044
   22   0017      0016
   24   0019      0018
   30   0020      0014
   40   0022      0043  0045
   45   0028      0027
   50   0029      0025
   55   0031      0030
   60   0044      0040
   70   0046      0022
```

Figure A-3 (Cont'd)